Accepted for publication in the AGU Geophysical Monograph volume titled "Understanding the Causes, mechanisms and extent of the Abrupt Climate Change" edited by Rashid, H., Polyak, L., and Mosley-Thompson, E.

A Review of Abrupt Climate Change Events in the Northeastern Atlantic Ocean (Iberian Margin): Latitudinal, Longitudinal and Vertical Gradients

Antje H. L. Voelker[1,2] and Lucia de Abreu[3]

1: Unidade de Geologia Marinha, Laboratorio Nacional de Energia e Geologia (LNEG), Estrada da Portela, Zambujal, 2610-143 Amadora, Portugal (antje.voelker@lneg.pt)
2: CIMAR Associate Laboratory, Rua dos Bragas 289, 4050-123 Porto, Portugal
3: former collaborator; Camberley, United Kingdom (luciaabreu@yahoo.com)

Abstract

The western Iberian margin has been one of the key locations to study abrupt glacial climate change and associated interhemispheric linkages. The regional variability in the response to those events is being studied by combining a multitude of published and new records. Looking at the trend from Marine Isotope Stage (MIS) 10 to 2, the planktic foraminifer data, conform with the alkenone record of *Martrat et al*. [2007], shows that abrupt climate change events, especially the Heinrich events, became more frequent and their impacts in general stronger during the last glacial cycle. However, there were two older periods with strong impacts on the Atlantic meridional overturning circulation (AMOC): the Heinrich-type event associated with Termination (T) IV and the one occurring during MIS 8 (269 to 265 ka). During the Heinrich stadials of the last glacial cycle, the polar front reached the northern Iberian margin (ca. 41°N), while the arctic front was located in the vicinity of 39°N. During all the glacial periods studied, there existed a boundary at the latter latitude, either the arctic front during extreme cold events or the subarctic front during less strong coolings or warmer glacials. Along with these fronts sea surface temperatures (SST) increased southward by about 1°C per one degree of latitude leading to steep temperature gradients in the eastern North Atlantic and pointing to a close vicinity between subpolar and subtropical waters. The southern Iberian margin was always bathed by subtropical water masses – surface and/ or subsurface ones –, but there were periods when these waters also penetrated northward to 40.6°N. Glacial hydrographic conditions were similar during MIS 2 and 4, but much different during MIS 6. MIS 6 was a warmer glacial with the polar front being located further to the north allowing the subtropical surface and subsurface waters to reach at minimum as far north as 40.6°N and resulting in relative stable conditions on the southern margin. In the vertical structure, the Greenland-type climate oscillations during the last glacial cycle were recorded down to 2465 m during the Heinrich stadials, i.e. slightly deeper than in the western basin. This deeper boundary is related to the admixing of Mediterranean Outflow Water, which also explains the better ventilation of the intermediate-depth water column on the Iberian margin. This compilation revealed that latitudinal, longitudinal and vertical gradients existed in the waters along the Iberian margin, i.e. in a relative restricted area, but sufficient paleo-data exists now to validate regional climate models for abrupt climate change events in the northeastern North Atlantic Ocean.

1. Introduction

The western Iberian margin is a focal location for studying the impact and intensity of abrupt climate change variability. Sediment cores retrieved there at a depth of more than 2200 m showed that the $\delta^{18}O$ of planktic foraminifer exhibits changes similar to those found in Greenland ice core records (e.g., $\delta^{18}O_{ice}$) whereas the $\delta^{18}O$ record of benthic foraminifer varies in a manner more reminiscent of the Antarctic temperature signal [*Shackleton et al.*, 2000]. Thus core sites retrieved at this margin allow studying interhemispheric linkages in the climate system. In addition, the southern edge of the North Atlantic's ice-rafted debris (IRD) belt [*Hemming*, 2004; *Ruddiman*, 1977] intercepted with the margin, so that melting icebergs reached the margin during Heinrich and Greenland stadials of the last glacial cycle and during ice-rafting events of preceding glacials [*Baas et al.*, 1997; *Bard et al.*, 2000; *de Abreu et al.*, 2003; *Moreno et al.*, 2002; *Naughton et al.*, 2007; *Sánchez-Goñi et al.*, 2008; *Zahn et al.*, 1997]. Following *Sanchez-Goñi and Harrison* [2010] who documented that on the Iberian margin the duration of the related surface water cooling and the Heinrich ice-rafting event *per se* can differ, Greenland stadials associated with Heinrich events are referred to as Heinrich stadials. Otherwise the Greenland stadial and Greenland interstadial nomenclature in this paper follows the INTIMATE group [*Lowe et al.*, 2001; 2008] and the *NGRIP members* [2004]. Only during Heinrich stadials did the Polar Front reach the Iberian margin [*Eynaud et al.*, 2009] associated with abrupt and intense cooling in the SST [*Bard et al.*, 2000; *Cayre et al.*, 1999; *de Abreu et al.*, 2003; *Martrat et al.*, 2007; *Naughton et al.*, 2009; *Vautravers and Shackleton*, 2006; *Voelker et al.*, 2006]. Using the records of three core sites, *Salgueiro et al.* [2010] were the first to show that while cooling was recorded at all sites during Heinrich events there existed a clear boundary between 40 and 38°N that not only affected the SST but also productivity. They attributed this boundary to a stronger influence of subtropical surface and subsurface waters in the southern region, which is in accordance with evidence from nannofossils [*Colmenero-Hidalgo et al.*, 2004; *Incarbona et al.*, 2010] and planktic foraminifer stable isotope data [*Rogerson et al.*, 2004; *Voelker et al.*, 2009]. *Voelker et al*. [2009] furthermore showed that upper water column stratification was diminished during the Heinrich events of MIS 2, especially along the western margin.

The Heinrich and Greenland stadials left their imprints also further down in the water column related to changes in the AMOC strength. One well documented change was the increased influence of lesser ventilated southern sourced waters, in particular the Antarctic Bottom Water (AABW), due to the shoaling of the interface between Glacial North Atlantic Intermediate Water (GNAIW) and AABW [*Margari et al.*, 2010; *Shackleton et al.*, 2000; *Skinner and Elderfield*, 2007; *Skinner et al.*, 2003] when AMOC was reduced or shut off. Along with this change ventilation of the deeper water column was reduced [*Baas et al.*, 1998; *Schönfeld et al.*, 2003; *Skinner and Shackleton*, 2004] and nutrient levels raised [*Willamowski and Zahn*, 2000]. In the mid-depth range another water mass is also important on the Iberian margin: the Mediterranean Outflow Water (MOW). Evidence for MOW changes mainly come from core sites in the Gulf of Cadiz, i.e. the southern margin. *Voelker et al*. [2006] showed that the lower MOW core reacted to abrupt climatic changes and was stronger during most parts of the Heinrich stadials and during Greenland stadials in accordance with evidence for deep convection in the Mediterranean Sea [*Kuhnt et al.*, 2008; *Schmiedl et al.*, in press; *Sierro et al.*, 2005]. Similar evidence also emerged for the upper MOW core [*Llave et al.*, 2006; *Toucanne et al.*, 2007] and for MIS 2 is has been shown that the MOW was not only strengthened, but settled significantly deeper – as deep as 2000 m – in the water column [*Rogerson et al.*, 2005; *Schönfeld and Zahn*, 2000]. Thus abrupt climatic changes affected all levels of the water column on the western Iberian margin.

During the last decades many cores have been retrieved from this region and studied in high-resolution but the records were seldom combined for a comprehensive regional reconstruction. In this review records from several cores are being compiled to look at regional variability in the response to abrupt climate change events and to trace latitudinal, longitudinal and vertical gradients during the last glacial cycle. All of this is important information needed for model/ data comparisons to validate how well climate models reproduce past conditions, e.g. [*Kjellström et al.*, 2010], and which local phenomena might have to be included in regional models to correctly represent the past conditions. Thus this study aims to describe how hydrographic conditions changed along with the abrupt climate events and to relate them the potential driving mechanisms. After having identified gradients during the last cycle their existence at the same position and with the same intensity during previous glacial cycles will be tested. Hereby one focus will be on the glacial upper water column structure as this will allow identifying boundaries between subpolar and subtropical dominated waters with implications for the position of hydrographic fronts.

2. Modern Hydrographic Setting

The western Iberian margin represents the northern part of the Canary/ Northwest African eastern boundary upwelling system and its upper water column hydrography is marked by seasonally variable currents and countercurrents (Fig. 1a). Upwelling and its associated features (Fig. 1b) dominate the hydrography generally from late May/ early June to late September/ early October [*Haynes et al.*, 1993] and is driven by the northward displacement of the Azores high-pressure cell and the resulting northerly winds. Intense upwelling on the western margin is linked to topographic features like Cape Finisterre, Cape Roca and Cape São Vicente (Fig. 1b) or submarine canyons [*Sousa and Bricaud*, 1992]. The Lisbon plume, linked to Cape Roca, can either extend westward as in Figure 1b or southward towards Cape Sines. During intense upwelling events, the filament off Cape S. Vicente extends southward and is fed by the Portugal Coastal Current (PCC; [*Fiúza*, 1984]). The more persistent feature, however, is an eastward extension of the filament along the southern Portuguese shelf break and slope [*Relvas and Barton*, 2002] where, when westerly winds prevail, the waters merge with locally upwelled waters (Fig. 1b).

The Portugal Current (PC), which branches of the North Atlantic Drift off Ireland, consists of the PC per se in the open ocean and the PCC along the slope during the upwelling season. The PC advects surface and subsurface waters slowly equatorward [*Perez et al.*, 2001; *van Aken*, 2001] and is centered west of 10°W in winter (Fig. 1a; [*Peliz et al.*, 2005]). The PC's subsurface component is the Eastern North Atlantic Central Water (ENACW) of subpolar (sp) origin, which is formed by winter cooling in the eastern North Atlantic Ocean [*Brambilla et al.*, 2008; *McCartney and Talley*, 1982]. The PCC, on the other hand, is a jet-like upper slope current transporting the upwelled waters southward [*Alvarez-Salgado et al.*, 2003; *Fiúza*, 1984]. At Cape S. Vicente, a part of this jet turns eastward and enters the Gulf of Cadiz [*Sanchez and Relvas*, 2003]. In the Gulf of Cadiz, it flows along the upper slope towards the Strait of Gibraltar [*Garcia-Lafuente et al.*, 2006], then called the Gulf of Cadiz Slope Current [*Peliz et al.*, 2007]. This current either forms an anticyclonic meander in the eastern Gulf of Cadiz or enters the Mediterranean Sea as Atlantic inflow [*Garcia-Lafuente et al.*, 2006; *Sanchez and Relvas*, 2003].

The Azores Current (AzC), another current branching of the Gulf Stream/ North Atlantic Drift, and the associated subtropical front reveal large meanders between 35 and 37°N in the eastern North Atlantic. While most of the AzC recirculates southward, its eastern branch flows into the

Gulf of Cadiz [*Johnson and Stevens*, 2000; *Peliz et al.*, 2005; *Vargas et al.*, 2003], where it feeds the offshore flow (Fig. 1a). Ocean models indicate that the AzC flow into the Gulf is quite significant [*Penduff et al.*, 2001] and link the existence of the current itself to the entrainment of surface to subsurface waters into the MOW [*Jia*, 2000; *Oezgoekmen et al.*, 2001]. Between October and March, when the Iberian Poleward Current (IPC; Fig. 1a), also a branch of the AzC, becomes a prominent feature off western Iberia, the thermal subtropical front (at ~17°C) is shifted northward and reaches the SW-Iberian margin [*Pingree et al.*, 1999]. Along with this shift AzC waters tend to recirculate from the Gulf of Cadiz into the region off Sines (Fig. 1a). *Peliz et al*. [2005] observe a recurrent frontal system, the Western Iberia Winter Front, which follows the thermal subtropical front in the south, but then meanders northward and separates the IPC from the PC (Fig. 1a). The IPC, extending down to 400 m, transports warm and salt-rich waters of subtropical origin [*Frouin et al.*, 1990; *Haynes and Barton*, 1990] and can be traced into the Bay of Biscay. The IPC's subsurface or undercurrent part conveys ENACW of subtropical (st) origin poleward year-round. $ENACW_{st}$, which is formed by strong evaporation and winter cooling along the Azores front [*Fiúza*, 1984; *Rios et al.*, 1992], is poorly ventilated, warmer and saltier than its subpolar counterpart. ENACW is the source for the water upwelled from May to September and in general $ENACW_{st}$ is upwelled south of 40°N and $ENACW_{sp}$ north of 45°N. In between either water mass can be upwelled depending on the strength of the wind forcing.

Between 500 and 1500 m, the water column along the western Iberian margin is dominated by the warm, salty MOW (Fig. 2) that is formed in the Gulf of Cadiz by mixing of Mediterranean Sea with Atlantic water, the above mentioned entrainment. Due to the mixing the MOW splits into two cores centered at about 800 and 1200 m [*Ambar and Howe*, 1979], which flow as undercurrents northward along the western Iberian margin. Facilitated by the margin's topography (e.g. canyons, capes, seamounts) the MOW cores shed many eddies [*Richardson et al.*, 2000; *Serra and Ambar*, 2002], called meddies, who greatly contribute to the MOW's admixing into the wider North Atlantic basin. Below the MOW at a depth around 1600 m Labrador Sea Water (LSW), the uppermost component of the North Atlantic Deep Water (NADW), can be found on the margin north of 40.5°N [*Alvarez et al.*, 2004; *Fiuza et al.*, 1998]. Deeper down in the water column Northeastern Atlantic Deep Water (NEADW) and Lower Deep Water (LDW) are found. LDW (> 4000 m) is warmed AABW that enters the eastern Atlantic basin through the Vema fracture zone at 11°N and the Iberian and Tagus abyssal plains partly as intensified current through the Discovery Gap near 37°N [*Saunders*, 1987]. The NEADW is a mixture between Iceland-Scotland Overflow Water, LSW, LDW and MOW with the contributions of LDW and MOW increasing to the south [*van Aken*, 2000]. The admixing of MOW into the NEADW explains why salinities (Fig. 2) and temperatures are higher in the eastern than in the western basin for equivalent depths down to 2500 m.

3. Material and Methods

Most of the records shown here are from Calypso piston cores retrieved with R/V *Marion Dufresne* II (IPEV) during the first IMAGES cruise in 1995 (MD95-) [*Bassinot and Labeyrie*, 1996], the fifth IMAGES cruise in 1999 (MD99-) [*Labeyrie et al.*, 2003], the Geosciences cruise in 2001 (MD01-), and the PICABIA cruise in 2003 (MD03-). Details on core locations and respective water depths are given in Table 1.

Planktic foraminifer census counts were done in the fraction >150μm. In general, SST data were calculated with the SIMMAX transfer function [*Pflaumann et al.*, 1996] using an extended (1066 samples) version of the *Salgueiro et al*. [2010] data base that is well suited for SST

reconstructions in the eastern North Atlantic. The additional samples are located mostly off NW Africa and for those cores for which we recalculated SST (MD95-2040, MD01-2443, MD01-2444, MD99-2339), interstadial and interglacial temperatures are often slightly (≈ 0.2°C) warmer than those previously published. We present only summer (July/ August/ September) temperatures (SST_{su}), but temperatures for the other seasons as well as the standard deviations derived from the minimum and maximum values of the selected nearest neighbors are available from the World Data Centre-Mare through the parent link http://doi.pangaea.de/10.1594/PANGAEA.737449. The methodical error for the SIMMAX based SST reconstructions is ± 0.8°C [*Salgueiro et al.*, 2010]. For core MD99-2331 and the MIS 3 section of core MD95-2042 SST values depicted in Figure 3 are from *Sánchez-Goñi et al.* [2008] and represent August SST. For core MD95-2042, the *Sánchez-Goñi et al.* [2008] August SST do not differ significantly from those obtained by *Salgueiro et al*. [2010] for the lower resolution counts done by *Cayre et al.* [1999], so that the records of MD95-2042 and MD99-2331 are comparable to the other ones shown in Figure 3.

Foraminifer based stable isotope data was measured either at Marum, University Bremen (Germany), in the Godwin Laboratory, Cambridge University (UK), in the Leibniz Laboratory for Radiometric Dating and Stable Isotope Research or at IfM-Geomar, the latter two in Kiel (Germany) (for details see original references listed in Table 1 and *Voelker et al.* [2009]). The benthic $\delta^{18}O$ record of core MD95-2040 combines values corrected to the *Uvigerina* level of the following foraminifer species: *Cibicidoides wuellerstorfi, Cibicidoides kullenbergi, Cibicidoides sp., Uvigerina peregrina, Uvigerina pygmea, Melonis sp.,* and *Globobulimina affinis* (only in MIS 6). Correction factors are those listed in *de Abreu et al.* [2005]. The benthic $\delta^{13}C$ record, on the other hand, only includes *Cibicidoides* derived values. For details on the MD01-2443 benthic records the reader is referred to *Martrat et al*. [2007].

Following *Voelker et al.* [2009] planktic foraminifer species for which stable isotope data were obtained for the MIS 3, 4 and 6 intervals are: *Globigerina bulloides; Globigerinoides ruber* white; *Neogloboquadrina pachyderma* (r) or (s); *Globorotalia inflata; Globorotalia scitula;* and *Globorotalia truncatulinoides* (r) or (s). *G. truncatulinoides* (s) values are generally only shown for MIS 4 when this species dominates over the right-coiling variety in the assemblage. For the MIS 3 section of core MD99-2339, on the other hand, samples of either coiling direction were analyzed and a combined record, sometimes based on mean values from double measurements, is shown. The combined $\delta^{18}O$ and $\delta^{13}C$ records for these species, which cover calcification depths from 50 to 400 m (see table 4 in *Voelker et al.* [2009]), are used to reconstruct conditions in the upper water column during the respective glacial intervals. Following *Ganssen and Kroon* [2000] the $\delta^{18}O$ difference between *G. bulloides* and *G. inflata* is used to evaluate seasonality. As discussed in *Voelker et al.* [2009] none of the planktic foraminifer isotope values are corrected because regional correction factors do not exist, yet.

Data and age models of cores MD95-2040, -2041, MD99-2336, -2339, MD01-2443 and -2444 used in this study are available from the WDC-Mare through the parent link http://doi.pangaea.de/10.1594/PANGAEA.737449.

4. Chronostratigraphies

For many of the cores, for which data from the last glacial cycle is shown, the (initial) age model was linked to the GISP2 ice core chronology either by direct tuning or by calibrating AMS ^{14}C ages with the *Hughen et al*. [2004] data. Because the focus of this study is on amplitudes and

timing between the different records rather than absolute ages GISP2 linked chronologies were kept instead of revising to NGRIP or Hulu Cave based calibration data. Thus, data of core MD95-2042 is shown on the *Shackleton et al*. [2000] chronology using the GISP2 correlation points, while cores MD99-2334K, MD99-2339, MD03-2698, and SU92-03 are shown on their original published timescales (Table 1). For MIS 3 data of core MD01-2444 correlation points to the GRIP chronology given by *Vautravers and Shackleton* [2006] were converted to GISP2 based ages. However, the alkenone derived SST record of this core is shown on the age scale of *Martrat et al*. [2007] in Figure 5, which is related to the NGRIP ice core on the GICC05 (back to 60 ka) and ss09sea chronologies for the last 120 ka. The age model of core MD95-2041, except for the MIS 2 section, where the age model of *Voelker et al*. [2009] is applied, was established by correlating its *G. bulloides* $\delta^{18}O$ record to the one of core MD95-2042 taking the positions of % *N. pachyderma* (s) maxima that are marking Heinrich stadials into account. The % *N. pachyderma* (s) maxima were especially relevant to identify Heinrich stadials 3 to 5 and 8. Also the age model for the MIS 4 section of core MD99-2336 is based on correlating its *G. bulloides* $\delta^{18}O$ record [*Llave et al.*, 2006] to core MD95-2042, while the MIS 2 section follows *Voelker et al.* [2009].

Data of core MD01-2443 is shown on the age model established by *Tzedakis et al*. [2009] who following *Shackleton et al*. [2000] tuned the benthic $\delta^{18}O$ record of this core to the δD record of the EPICA Dome C ice core on its EDC3 chronology. *Salgueiro et al.* [2010] recently published a chronology of core MD95-2040 back to the top of MIS 6. However, when compiling the figures for this paper, we noted that with the *Salgueiro et al.* [2010] age model the % *N. pachyderma* (s) maximum/ SST minimum of Heinrich stadial 8 is significantly older than the one in core MD95-2042. Thus a revised stratigraphy for MIS 4 and late 5 was established by correlating the *G. bulloides* $\delta^{18}O$ records of cores MD95-2040 and MD95-2042. Stratigraphic control within MIS 6 follows *Margari et al*. [2010] whereas for the section older than MIS 6 the new benthic $\delta^{18}O$ record was tuned to the LR04 stack [*Lisiecki and Raymo*, 2005]. The core now has a bottom age of 360 ka (MIS 10/ 11 boundary) that is significantly younger than the age obtained by *Thouveny et al*. [2004] through extrapolation.

5. Surface water gradients and implications for the Polar Front position

5.1. Conditions during the last 80 ka

The compilation of the existing high-resolution planktic foraminifer derived SST and % *N. pachyderma* (s) records (Fig. 3) visibly reveals the strong impact the Heinrich stadials had in this region and the temperature gradients that existed within a latitudinal band of only seven degrees. The Heinrich stadials are clearly distinguished by maxima in % *N. pachyderma* (s) and the coldest SST in all records. The coldest SST during Heinrich and Greenland stadials were recorded at the two northernmost sites SU92-03 and MD99-2331 with SST_{su} in the range of 4 to 6°C during the Heinrich stadials. Cooling at these sites occurred during the whole period of a Heinrich stadial and % *N. pachyderma* (s) generally exceeded 90%, values today associated with polar water masses [*Eynaud et al.*, 2009]. While these values are the coldest/ highest in our compilation, conditions were more extreme just two degrees further to the north in the Bay of Biscay [*Sánchez-Goñi et al.*, 2008; *Toucanne et al.*, 2009] where % *N. pachyderma* (s) were close to 100% during the Heinrich stadials and most Greenland stadials. If one compares the records of cores MD99-2331 and MD95-2040 (Fig. 3), also separated by about two degrees latitude, another gradual change appears. At the latter site at 40.6°N maximal percentages of *N. pachyderma* (s) were more in the range of 80 to 90% resulting in two degrees warmer surface waters. Despite the warmer conditions at site MD95-2040, the overall shape in the % *N. pachyderma* (s) and SST

curves is similar in the three sites north of 40°N setting them apart from the ones further to the south and confirming the hydrographic boundary between 40 and 38°N described by *Salgueiro et al*. [2010] as a robust feature.

South of 38°N the % *N. pachyderma* (s) values – with the exception of one data point during Heinrich stadial 4 in core MD01-2444 – did not exceed 60% (Fig. 3) and coldest SST during Heinrich stadials were in the range of 8 to 10°C, i.e. two or more degrees warmer than at site MD95-2040. The % *N. pachyderma* (s) values are those associated with arctic waters in the Nordic Seas [*Eynaud et al.*, 2009] but the reconstructed SST values are more in the range of the modern subpolar gyre. Nevertheless, the data clearly shows that the arctic or even subarctic front was located in the range of 39°N during Heinrich and Greenland stadials, while the hydrographic polar front seems to have been located somewhere close to 41°N [*Eynaud et al.*, 2009]. Such a close spacing of hydrographic fronts, but on a more longitudinal scale, is today observed off New Foundland and in the Norwegian Sea [*Dickson et al.*, 1988], i.e. in regions where Atlantic surface waters come in close vicinity to (sub)polar waters. On the latitudinal scale such steep temperature gradients are known from the last glacial maximum (LGM) [*Pflaumann et al.*, 2003]. The front near 39°N would generally mark the southern edge of the Heinrich IRD belt, in accordance with evidence from the western basin [*Hemming*, 2004], but this does not mean that icebergs did not cross this boundary and deposited their IRD further to the south [*Bard et al.*, 2000; *Toucanne et al.*, 2007; *Voelker et al.*, 2006; *Zahn et al.*, 1997]. From the % *N. pachyderma* (s) records, however, is becomes quickly obvious that Heinrich stadials 1, 4 and 6 had a stronger impact on the hydrography in the Sines region than in the Gulf of Cadiz (site MD99-2339; Fig. 3) where % *N. pachyderma* (s) values were significantly lower (< 16%).

Even smaller scale regional differences can be investigated using the three records off Sines (MD95-2041, MD95-2042, MD01-2444; Fig. 3). The two core sites at 10°W, i.e. further offshore, tend to record slightly warmer SST not only during the cold climate events but also during some Greenland interstadials (for an explanation see chapter 5.2). Especially site MD01-2444 reveals warmer SST during the Greenland interstadials indicating that this site was more strongly influenced by subtropical Azores Current waters than the other two sites –either from being located underneath a northward extending meander of the Azores front or from being influenced by a paleo-IPC (Fig. 1a). Sporadically the SST were even warmer than those recorded further to the south at site MD99-2339. On the other hand, sites MD01-2444 and MD99-2339 experienced the colder conditions during the first half of Greenland interstadial 8 more strongly than sites MD95-2042 and MD95-2041. This cooling was more pronounced at the three northern sites (MD95-2040, MD9-2331, SU92-03; Fig. 3) and must therefore have been advected from the north to the south, most likely with the more offshore located Portugal Current. Thus high regional variability linked to the position and shape of fronts and/ or upwelling system dynamics also occurred under glacial climate conditions and needs to be taken into account when impacts of abrupt climate change are discussed and compared to climate model results.

In summary, the core transect along the western Iberian margin reveals that during the Heinrich and Greenland stadials of the last 80 ka, SST increased from north to south by about 1°C along with a latitudinal shifts of about one degree. During Heinrich events, SST_{su} minima were around 4°C between 42 and 43°N, near 6°C at 40.6°N, between 8 and 9°C near 38°N, and near 10°C at 36°N. The polar front was most likely located near 41°N and the (sub)arctic front with the atmospheric Polar Front at about 39°N. In accordance with the temperature gradients and frontal positions, climate conditions were more severe in the north than in the south with subsequent

impacts on the vegetation [*Fletcher et al.*, 2010; *Naughton et al.*, 2009; *Roucoux et al.*, 2005; *Sánchez-Goñi et al.*, 2008]

5.2 Longitudinal Differences off Sines – 38°N: The upwelling influence

The above mentioned upwelling system dynamics that might drive regional variability off the Sines coast can best be seen by comparing the records of cores MD95-2042 and MD95-2041 (Fig. 4). The *G. bulloides* $\delta^{18}O$ record of core MD95-2041, located closer to the coast (Fig. 1a), differs from the one of MD95-2042, especially during MIS 3, with a less clear imprint of Greenland stadial and interstadial cycles. Thus at site MD95-2041 a different hydrographic signal was recorded. The $\delta^{13}C$ and SST records further support this. Site MD95-2041 experienced a much higher SST_{su} variability with frequent short to longer lasting coolings in the range of 3 to 6°C between the Heinrich stadials (Fig. 4e); a variability that persists in relation to the higher resolution SST_{Aug} record of *Sánchez-Goñi et al.* [2008] for core MD95-2042 shown in Figure 3. Along with the colder SST, *G. bulloides* $\delta^{13}C$ values are generally higher at site MD95-2041 than at MD95-2042 (Fig. 4c). If one excludes temperature [*Bemis et al.*, 2000] as cause, the difference would indicate that nutrient concentrations were lower in the nearshore waters. Fewer nutrients together with the SST variability indicate that site MD95-2041 experienced periods of intense upwelling in the intervals between the Heinrich stadials with the associated high surface water productivity depleting the nutrients. Today site MD95-2041 is more strongly influenced by the filament often extending southward from Lisbon than site MD95-2042 and during glacial times, when due to the lower sea level the coastline was displaced further offshore, also the local upwelling along the Sines coast (Fig. 1b) would be in the vicinity of site MD95-2041. High glacial productivity at this site outside of the ice-rafting events of MIS 2 was also observed by *Voelker et al*. [2009]. In consequence, these two closely spaced sites reveal that a local phenomenon like upwelling can strongly modify the paleo-data and result in locally different signals that are not related to the millennial-scale climate variability.

5.3 Comparison between the last and previous glacial cycles

To verify if the temperature gradients described in chapter 5.1 and the associated frontal positions also existed during previous glacials we are using the records of core MD95-2040, the site located north of the front, and spliced records from the offshore sites off the Sines coast (Fig. 5). The planktic and benthic stable isotope records indicate that both sites reliably recorded the glacial/ interglacial cycles and experienced millennial-scale variability in the surface and deep-water hydrography.

The % *N. pachyderma* (s) and SST_{su} records of core MD95-2040 clearly indicate that glacial MIS 6 differed not only in absolute values but also in the intensity (% *N. pachyderma* (s); SST) of the abrupt climate change variability as previously described by *de Abreu et al*. [2003]. MIS 6 % *N. pachyderma* (s) values in core MD95-2040 are comparable to the levels recorded in the cores off Sines during the last glacial cycle, meaning SST were significantly warmer. Although hampered by a data gap the same can be said for the Sines area where % *N. pachyderma* (s) values were about half of those of core MD95-2040 (Fig. 5d), especially during Heinrich event 11, and more in the range of the core MD99-2339 during Heinrich stadial 4 (Fig. 3). Thus a boundary again existed between 38 and 40°N, but this time it was clearly the subarctic front. Percent *N. pachyderma* (s) values during Heinrich event 11 reached 90% at site SU92-03 [*Salgueiro et al.*, 2010] and 100% in the Bay of Biscay [*Toucanne et al.*, 2009]. So the polar front still reached the Iberian margin but only in the northernmost ($\geq$ 43°N) section and was located further to the north than during the last glacial cycle.

For glacial MIS 8, data for core MD95-2040 exists only between 253 and 266 ka. Within this interval % *N. pachyderma* (s) levels exceeded 70% and reached 90%; thus were in the range of those recorded during the Heinrich stadials of the last glacial cycle. Conditions stayed cold for an extended period (261.6 – >266 ka), lasting longer than a typical Heinrich event. Long lasting cold was also recorded in the Bay of Biscay [*Toucanne et al.*, 2009], mostly with levels close to 100% *N. pachyderma* (s) and reminding of the hydrographic conditions observed for the Heinrich stadials. Within age constraints this interval coincided with a Heinrich-type ice rafting event recorded at IODP Site U1308 [*Hodell et al.*, 2008], so that similar forcing mechanisms and responses in the AMOC can be assumed. The low benthic $\delta^{13}C$ values recorded at sites MD95-2040 and MD01-2443 (Fig. 5f) between 271 and 262 ka clearly indicate that the AMOC was reduced or shut off. The more depleted signal recorded in core MD95-2040 is most likely related to marine snow [*Mackensen et al.*, 1993] during a period of high productivity [*Thomson et al.*, 2000]. In comparison to the northern areas cooling in the surface waters off Sines was reduced – similar to the previous glacials – but this time the peak cooling in the south was significantly shorter in the planktic foraminifer records (Fig. 5c, d). Its duration was, however, comparable in the alkenone SST record (Fig. 5b) indicating decoupling in the response of the two plankton groups. On the other hand, the second abrupt cold event within MIS 8 (242.5 – 246.5 ka) is only evident in the foraminifer records and not in the alkenone SST. This event, associated with Termination III, had a lesser impact on the AMOC because the benthic $\delta^{13}C$ values were less depleted and thus indicate a GNAIW/ AABW boundary deeper in the water column than during the previous event.

During glacial MIS 10 only the Heinrich-type event associated with Termination IV [*Hodell et al.*, 2008; *Stein et al.*, 2009] had a pronounced impact on the hydrography off Iberia. The percent *N. pachyderma* (s) levels at site MD01-2443 were again lower than during the last glacial cycle and during the MIS 8 Heinrich-type event (Fig. 5d), but comparable to Heinrich event 11. The benthic $\delta^{13}C$ levels at both sites were, however, similar to the MIS 8 event (Fig. 5f) and again indicate a much reduced AMOC and a modified signal at site MD95-2040 due to high productivity [*Thomson et al.*, 2000]. Including evidence from other cold stages such as MIS 7d it is clear that a boundary – sometimes the arctic, sometime the subarctic front – always separated the two core sites during abrupt cooling events. The longer records show moreover that the strong coolings associated with the Heinrich stadials of the last glacial cycle were close to unique and had only two counterparts during the last 420 ka.

6. Impacts on the glacial upper water column

6.1. The last glacial cycle: MIS 4 and MIS 2

Abrupt climate events not only affected the uppermost waters but also left their imprints in the subsurface waters [*Rashid and Boyle*, 2007; *Voelker et al.*, 2009], information on which is often sparse. The structure of the water column from 0 to about 400 m can be investigated by combining the isotope data of various planktic foraminifer species (for details see table 4 in *Voelker et al*. [2009]). Here we focus on the last three glacial periods but using the MIS 2 data only for comparison because they have been discussed in detail by *Voelker et al*. [2009]. Data from north of the front existing between 38 and 40°N, i.e. core MD95-2040, is compared to records from south of the front, i.e. core MD95-2041 for the last glacial cycle and core MD01-2443 for MIS 6. One peculiarity associated with the deep dwelling foraminifers used is the dominant coiling direction of *G. truncatulinoides*. During MIS 2 and 6 the right coiling variety, which is known from just one geno-type [*de Vargas et al.*, 2001], dominated, while during MIS 4

the left coiling variety that can be attributed to all four known geno-types is more abundant. Since the geno-type often found in the subtropical of waters of the Sargasso and Mediterranean Sea [*de Vargas et al.*, 2001] is the only one with both coiling directions, we assume that our species belong to the same geno-type.

The hydrography during the glacial maxima of MIS 2 and 4 at site MD95-2040 was similar (Fig. 6) with the IPC, as indicated by the *G. ruber* white values, being absent during the latest part and during the deglaciations, i.e. Heinrich stadials 1 and 6, respectively. The interval when *G. ruber* white was absent during late MIS 4 is also the one when *N. pachyderma* (s) and thus subpolar waters were continuously present. Along with the rise in % *N. pachyderma* (s), just prior to Greenland interstadial 18, seasonality ($\Delta\delta^{18}O$; Fig. 6d) increased, but the highest seasonal contrast was associated with Heinrich stadial 6. Then seasonality was in the same range as the values observed during the MIS 2 Heinrich stadials. Greenland interstadial 18 was associated with warming (lower $\delta^{18}O$ values) in the surface to subsurface waters shown in particular by *G. bulloides*, *N. pachyderma* (r) and *G. inflata* (Fig. 6a, b). The earlier Greenland interstadials 19 and 20 are poorly resolved, but the presence of *G. ruber* white and reduced seasonality indicates relative warm and stable conditions. This constancy also referred to the subsurface waters as indicated by the relative stable $\delta^{18}O$ records of *G. inflata* and *G. truncatulinoides* (Fig. 6b). The MIS 4 deep dweller records are clearly different from MIS 2 when extremely light values were measured [*Voelker et al.*, 2009]. During this early part of MIS 4 the subsurface waters were well ventilated, especially the $ENACW_{st}$ recorded in the *G. truncatulinoides* $\delta^{13}C$ values (Fig. 6e). We relate the *G. truncatulinoides* data of core MD95-2040 to the $ENACW_{st}$, and thus a signal transported northward, because of the similar isotopic levels observed in both MD95-2041 (Fig. 7e) and MD95-2040. The good ventilation in the subsurface waters is also common to both glacial periods. Another difference to MIS 2 or more specifically to the younger Heinrich stadials at site MD95-2040 is, however, that *G. inflata* was present during some intervals of Heinrich event 6 with the light $\delta^{18}O$ values pointing to lower salinities in the subsurface waters.

South of the arctic front at site MD95-2041 (Fig. 7), the planktic $\delta^{18}O$ and for *G. bulloides* and *N. pachyderma* (r) also the $\delta^{13}C$ records show distinct millennial-scale oscillations that were related to the Greenland stadial/ interstadial cycles 18 to 20. During all the interstadials warming is observed in the surface to subsurface waters (Fig. 7a, b). Conditions in the subsurface waters appear to have been very stable and the $\delta^{18}O$ values of all three deep dwelling species were close together (Fig. 7b). Thus subsurface water conditions on the southwestern Iberian margin were more stable during MIS 4 than during MIS 2. Seasonality (Fig. 7d) seems to have been a bit more variable at site MD95-2041 than at MD95-2040 and increased during Greenland stadial 19. During this stadial, % *N. pachyderma* (s) rose slightly (Fig. 7c) and $\delta^{13}C$ of *N. pachyderma* (r) and *G. bulloides* (Fig. 7f) indicated fewer nutrients in the surface waters. Since this site was highly influenced by upwelling with increased productivity during some of the MIS 2 stadials [*Voelker et al.*, 2009], all these signals are interpreted as being upwelling related.

Overall, hydrographic conditions north and south of the front were similar during MIS 4 and 2, respectively. Differences between the two glacial periods were more restricted to the subsurface waters, especially the $ENACW_{st}$, where conditions were more stable during the older glacial period. The presence of $ENACW_{st}$ and in sections also of *G. ruber* white indicate that Azores Current derived waters were present during much of the glacial periods, even if potentially restricted to a circulation pattern similar to the modern winter circulation (Fig. 1a). This further

implies that the Azores Front most likely extended towards the southern Iberian margin during both MIS 2 [*Rogerson et al.*, 2004] and 4 and might be the front observed between 38 and 40°N.

6.2 The penultimate glacial – MIS 6

As already indicated by the % *N. pachyderma* (s) evidence discussed in chapter 5.3 MIS 6 differed from the two younger glacial periods. This is further supported by the multi-species stable isotope evidence of cores MD95-2040 (Fig. 8) and MD01-2443 (Fig. 9). The subtropical species *G. ruber* white was always present at the southern location and nearly continuously also at site MD95-2040 indicating a northward heat transport stronger than during the last glacial cycle. This heat flux most likely occurred with the IPC, similar to the LGM [*Eynaud et al.*, 2009; *Pflaumann et al.*, 2003; *Voelker et al.*, 2009]. Ventilation of those waters was, however, highly variable (Fig. 8e), much more so than during any of the younger glacial periods. Seasonality variations (Fig. 8d), on the other hand, were much higher than during MIS 2 and 4 (Fig. 6d). Seasonal contrasts were driven by the relatively more stable conditions in the winter mixed layer (Fig. 7b). Longer lasting seasonality extremes were associated with Heinrich event 11, similar to the younger Heinrich stadials, and occurred during the intervals from 158.9 to 163 ka and 168.2 to 173.2 ka while shorter oscillations marked the beginning of MIS 6 (177 – 188 ka; Fig. 8d). In particular the interval from 158.9 to 163 ka was associated with higher abundances of *N. pachyderma* (s) (Fig. 8c), the presence of ice-rafted debris [*de Abreu et al.*, 2003] and a reduced tree cover on land [*Margari et al.*, 2010] supporting relative harsher climate conditions.

As described for the previous glacial periods conditions on the southwestern Iberian margin were more stable (Fig. 9). The *G. truncatulinoides* $\delta^{18}O$ record shows hardly any change and the respective $\delta^{13}C$ values indicate a well-ventilated $ENACW_{st}$ (Fig. 9d), in contrast to the subtropical surface waters reflected in the *G. ruber* white $\delta^{13}C$ values. Millennial-scale oscillations were limited and restricted to the earlier part of MIS 6. However, the two older cooling events within MIS 6e had no major impact on the water column structure and the nearly flat *G. truncatulinoides* $\delta^{18}O$ record indicates that conditions must have been similar to the ones of the penultimate glacial maximum (Fig. 9b). In the $ENACW_{st}$ the most pronounced changes occurred between 153 and 161 ka, when ventilation was reduced and and *G. truncatulinoides* $\delta^{18}O$ values were lower. It needs to be seen in the future if these lighter $\delta^{18}O$ values were a temperature and/or salinity signal. Overall, the same picture as for the previous glacial periods emerges with the southern area being strongly affected by subtropical waters and the Azores Front located nearby. This clearly indicates that this pattern is a robust feature independent of the overall climate forcing.

7. Imprints throughout the whole water column

As mentioned in the introduction the impacts of the abrupt climate change events can be traced down into the intermediate and deep water levels. To emphasize this records from cores off the Sines coast or in the Gulf of Cadiz are combined in Figures 10 and 11. The hydrographic evidence for the last 65 ka is based on planktic and benthic foraminifer $\delta^{18}O$ data, the mean grain size as evidence for MOW variability and deep-water temperature (DWT) records. Ventilation status (Fig. 11) is assessed from planktic and benthic $\delta^{13}C$ records.

7.1 Hydrography

The records clearly shows that the Greenland-type millennial-scale variability impacted the complete water column from the sea surface down to 2465 m, i.e. the water depth of site MD01-2444. The planktic foraminifer records all show warming (interstadial) and cooling (stadial)

cycles that were contemporary in the water depths from 0 to 400 m with similar amplitudes in the *G. bulloides* (Fig. 10c) and *G. truncatulinoides* (Fig. 10d) records and a smaller amplitude in the *G. ruber* white data (Fig. 10b). The *G. truncatulinoides* data of core MD99-2336 from the southern Portuguese margin (gray lines in Fig. 10d) even indicate the presence of subtropical ENACW in the region during Heinrich stadials 1 and 6, in accordance with nannofossil evidence, i.e. maxima of the subtropical, deep dwelling coccolithophore *F. profunda* [*Colmenero-Hidalgo et al.*, 2004; *Incarbona et al.*, 2010]. The presence of *G. ruber* white during these periods (Fig. 10b) even points to the presence of subtropical surface waters [*Voelker et al.*, 2009]. The stadial/ interstadial cyclicity is also recorded in the MOW strength (Fig. 10e) with enhanced bottom current speeds (higher mean grain size values) during the cold periods [*Voelker et al.*, 2006]. Temperatures in the upper NADW (Fig. 10f; [*Skinner and Elderfield*, 2007]) generally also follow the Greenland-type pattern with warmer DWT during the interstadials and colder ones during the stadials as to be expected by changes in NADW or AABW predominantly bathing the site, respectively. The DWT record of site MD01-2444, however, also shows short-term warming events during Heinrich stadials 4 and 5 that *Skinner and Elderfield* [2007] attribute to the potential admixing of MOW, which similar to the last deglaciation could have reached as deep down as 2200 m on the Sines margin [*Schönfeld and Zahn*, 2000]. Admixing of deeper flowing MOW into depths of 2465 m could also explain some of the signals seen in the benthic stable isotope records of core MD95-2040 (Fig. 5e, f) further to the north. The shift from a Greenland- to an Antarctic-type climate signal occurred somewhere between 2500 and 3100 m water depth where the benthic $\delta^{18}O$ signal of core MD95-2042 (Fig. 10h; [*Shackleton et al.*, 2000]) clearly reflects the oscillations depicted in the EDML ice core record (Fig. 10i; [*EPICA Community Members*, 2006]). The GNAIW/ AABW boundary was therefore located deeper in the water column off southern Iberia than in the western Atlantic basin [*Curry and Oppo*, 2005] and the northeastern Atlantic [*Sarnthein et al.*, 2001], most probably due to the presence of the deeper flowing MOW.

7.2. Water column ventilation

In the upper 400 m of the water column, nutrient levels and thus ventilation of the respective water mass (Fig. 11b-d) were not driven by the millennial-scale variability seen in the $\delta^{18}O$ records. For *G. ruber* white glacial values tend to be lower than the Holocene ones reflecting the oligotrophic waters in the central Gulf of Cadiz. During the glacial and deglacial section the lower values probably mirror local conditions with periods of stronger winter mixing, the time for refurbishing nutrients in the Gulf of Cadiz [*Navarro and Ruiz*, 2006]. For *G. bulloides* the trend is opposite with higher values during the glacial. Since the *G. bulloides* record is from core MD95-2042 off Sines and thus from a region potentially experiencing upwelling the *G. bulloides* $\delta^{13}C$ record was most likely modified by the productivity conditions in this region. Glacial productivity – and thus nutrient consumption – was higher in this region than during the Holocene [*Salgueiro et al.*, 2010]. The glacial subthermocline waters (100 – 400 m) were mostly well ventilated and contained few nutrients hinting to $ENACW_{st}$ as prevailing water mass. Only during Heinrich stadials 1 and 4 lower $\delta^{13}C$ values were recorded that could indicate that either less ventilated $ENACW_{sp}$ penetrated into the Gulf of Cadiz along with the melting icebergs [*Voelker et al.*, 2006] or that Antarctic Intermediate Water (AAIW) was mixed into the subtropical ENACW. Small amounts of AAIW can be found in the Gulf of Cadiz waters today [*Cabeçadas et al.*, 2003] and paleoceangraphic studies have shown that AAIW penetrated further northward during glacial times [*Pahnke et al.*, 2008].

Millennial-scale oscillations in the ventilation of the water column were finally recorded in the intermediate to bottom waters, i.e. those water masses directly reflecting the status of the overturning circulation either in the Mediterranean Sea or in the Atlantic Ocean (Fig. 11e-h). The record of core MD99-2339 bathed by the lower MOW core (Fig. 2, 11e) shows clear cyclicity with relatively poorer ventilation during the Greenland interstadials and better during the Greenland stadials [*Voelker et al.*, 2006], similar to the pattern observed for the Western Mediterranean Deep Water [*Cacho et al.*, 2000; *Sierro et al.*, 2005]. Records from the Mediterranean Sea's eastern and western basins indicate that intermediate and deep waters were well oxygenated during Greenland stadials and during the greater parts of the Heinrich stadials [*Bassetti et al.*, 2010; *Cacho et al.*, 2000; *Schmiedl et al.*, in press; *Sierro et al.*, 2005]. Thus the poor ventilation of the MOW during the Heinrich stadials must result from the admixing of poorly ventilated Atlantic waters such as the $ENACW_{st}$ reflected in the *G. truncatulinoides* data (Fig. 11d) and potentially also AAIW. In the upper NADW/ GNAIW level at 2465 m (Fig. 11e) and deeper down the ventilation status was primarily driven by the well known up and down movement of the NADW/ AABW interface with better ventilation (= NADW) during the interstadials, when AMOC was strong, and poorer ventilation during the stadials (= AABW). When NADW was present benthic $\delta^{13}C$ values were similar from 2465 to 3146 m water depth and during glacial times also not much different at 4602 m (Fig. 11f-h) indicating a homogeny in the deeper water column during the interstadials that is also seen today [*Alvarez et al.*, 2004]. During the LGM and most Heinrich stadials the 2465 m data shows, however, excursions to higher $\delta^{13}C$ values that were in the range of those recorded in the lower MOW core at site MD99-2339 (Fig. 11e, f). Thus the benthic $\delta^{13}C$ data confirms what the DWT already implied: the deeper flowing MOW was admixed into the GNAIW and led sometimes to a better ventilation of the intermediate-depth water column along the western Iberian margin. Extremely low benthic $\delta^{13}C$ values, on the other hand, were recorded at 4602 m during MIS 2 and 4 (Fig. 11h). This record is from core MD03-2698 [*Lebreiro et al.*, 2009] located in the Tagus abyssal plain and shows that bottom waters in this deep basin were hardly renewed during the glacial maxima. Even today the deep abyssal plains off Iberia can only be ventilated by flows through a few deep gaps [*Saunders*, 1987]. However, additional modification of the benthic $\delta^{13}C$ signal due to remineralization of organic matter transported down the canyons by the frequent turbidites [*Lebreiro et al.*, 2009] could also have played a role.

8. Conclusions

The combination of various high-resolution records allowed studying how events of abrupt climate change affected the water column along the western Iberian margin and which latitudinal and vertical boundaries existed. The abundance of records from the Sines region on the southwestern margin, furthermore, permitted to assess signal modification due to upwelling.

The surface water records from the Iberian margin clearly reveal that two fronts intercepted with the margin during the Heinrich stadials of the last glacial cycle and during extreme cold events of previous glacial periods. During the last glacial cycle, the polar front was located near 41°N leading to the harshest climate conditions in the northern regions. The arctic front was located about two degrees further to the south, near 39°N and might have coincided with the Azores Front. The latitudinal positioning of these fronts led to steep temperature gradients along the margin with SST_{su} increasing by 1°C per degree of latitude, i.e. from 4°C at 42°N to 10°C at 36°N. The foraminifer data furthermore showed that Heinrich events became more frequent and had stronger hydrographic impacts during the last glacial cycle. Similar events were recorded only with Heinrich event 11 during Termination II and along with the Heinrich-type events

during early MIS 8 and Termination IV. MIS 6 was overall a warm glacial with subtropical waters dominating the hydrography along the southern Iberian margin and penetrating at least as far north as 40.6°N during much of the period. Hydrographic conditions north and south of the 39°N boundary were in general similar during MIS 2 and 4, but MIS 4 like MIS 6 seems to have more strongly been affected by subtropical subsurface waters. MIS 6, however, differed from its younger counterparts in regard to the increased seasonality and the extreme variations in the nutrient level of the subtropical surface waters.

Because the western Iberian margin is an upwelling area, upwelling can always affect the climate records. A clear indication for upwelling events modifying climate records and thus leading to different paleo-data for the same events in close vicinity is given by the differences observed between cores MD95-2041 and MD95-2042 on the Sines coast. Core MD95-2041, located closer to the coast, experienced much more variability in its *G. bulloides* stable isotope records that can only be explained by upwelling. Upwelling also seems to be driving some of the variations observed in the planktic stable isotope records of core MD95-2040 during MIS 6.

A second "local" hydrographic phenomenon affecting the water column in the eastern North Atlantic is the MOW. During glacial times and especially the Heinrich events and Greenland stadials the MOW settled deeper in the water column allowing it to be admixed into the intermediate-depth water masses. Thus records from 2465 m water depth indicate imprints of MOW by warming events – so far confirmed for Heinrich events 4 and 5 – and by a better ventilation of these water depths relative to the western basin. Due to the admixing the boundary between GNAIW and AABW was located between 2465 and 3100 m on the Iberian margin. As consequence Greenland-type climate oscillations can be traced down to this level, while the deeper sites follow the Antarctic-type of climate change. The deepest basins on the Iberian margin apparently experienced periods of reduced water mass renewal during MIS 2 and 4.

For the last glacial cycle we now have a comprehensive picture regarding latitudinal and vertical gradients in the water column along the Iberian margin and it is hoped that the existing data can serve as grounds for regional climate models of abrupt climate change events.

Acknowledgements

We are indebted to Yvon Balut, IPEV and the crew of RV *Marion Dufresne* as well as the IMAGES project for the recovery of excellent core material. The EU Access to Research Infrastructure PALEOSTUDIES program is acknowledged for the financial support that allowed the multi-species stable isotope analyses. Monika Segl and the Geosciences Dept. (FB 5) of the Univ. Bremen is thanked for hosting A. V. and L. A. during their respective PALEOSTUDIES stays. Additional thanks for excellent stable isotope results go to Helmut Erlenkeuser (Leibniz Labor, Univ. Kiel) and Mike Hall and James Rolfe (Godwin Lab., Univ. Cambridge). A. Rebotim is thanked for her help in completing the benthic isotope records of core MD95-2040. The Fundação de Ciência e Tecnologia (FCT) supported this research through the MOWFADRI and SEDPORT projects and postdoctoral fellowships to A. V. and L. A. A. V. furthermore acknowledges her Ciência 2007 grant. Finally, L. A. would like to remember all the dedication, incentive and enthusiasm of the late Nick Shackleton and his guidance and collaboration throughout many of the studies involving these particular Iberian Margin cores.

Figure Captions:

Figure 1. a) Map of the western Iberian margin with core sites and surface water circulation in winter as summarized by *Peliz et al*. [2005]. The location of core MD95-2039 (circle filled in white), which is mentioned in the text but for which no data is shown, is also indicated. b) NASA Aqua MODIS satellite derived chlorophyll a picture (http://oceancolor.gsfc.nasa.gov/FEATURE/gallery.html) for 13th September 2005 showing the regions most affected by upwelling along the Iberian margin and the extensive filaments off Capes Finisterre, Roca and São Vicente. Dots mark the same core locations as in a) (except for MD95-2039).

Figure 2. Salinity profile of WOCE transect A3 [*Schlitzer*, 2000] (http://www.ewoce.org/) with dots marking from top to bottom depths of core sites MD99-2336, MD99-2339 (both not on correct longitude), MD01-2444, MD95-2042/ MD99-2334K, and MD03-2698. Water mass abbreviations are: ENACW: Eastern North Atlantic Central Water; MOW: Mediterranean Outflow Water; NADW: North Atlantic Deep Water; NEADW: Northeastern Atlantic Deep Water; AABW: Antarctic Bottom Water; LDW: Lower Deep Water.

Figure 3. Latitudinal gradients in the abundance of % *N. pachyderma* (s) (%; left column) and sea surface temperature (SST) derived from planktic foraminifer assemblages (°C; right column) over the last 80 ka. SST values refer to summer (black) or August (gray). The transect from north to south consists of cores SU92-03 [*Salgueiro et al.*, 2010]; MD99-2331 [*Sánchez-Goñi et al.*, 2008]; MD95-2040 [*de Abreu et al.*, 2003] with SST recalculated for this study; MD95-2041 [*Voelker et al.,* 2009; this study]; MD95-2042 with SST recalculated based on counts of *Cayre et al*. [1999] (black SST line and % *N. pachyderma* (s)) and SST data from *Sánchez-Goñi et al.* [2008] (gray line); MD01-2444 [*Vautravers and Shackleton*, 2006] with SST recalculated for this study; and MD99-2339 [*Voelker et al.,* 2006; 2009; this study]. Note the change in the % *N. pachyderma* (s) scale for core MD99-2339 to adjust for the gradient of more than 90% in the north to the maxima of just 16% in the south. A shift by 2°C in the SST scale is also observed for core MD95-2041 and the records below. Gray bars mark Heinrich stadials.

Figure 4. Longitudinal gradients in surface water properties off Sines between offshore site MD95-2042 (10.17°W; gray lines; [*Cayre et al*., 1999; *Shackleton et al*., 2000; SST: *Salgueiro et al*., 2010]) and nearshore site MD95-2041 (9.52°W; black lines; [*Voelker et al.,* 2009; this study]). Panels a) and b) show the respective *G. bulloides* $\delta^{18}O$ records and c) and d) the *G. bulloides* $\delta^{13}C$ records with the gray shading in c) representing the offset between the two records. Panel e) shows the two foraminifer-based summer SST records. H1 to 8 mark Heinrich stadials 1 to 8 and GI Greenland interstadials, respectively.

Figure 5. Latitudinal gradients in surface and deep-water properties between the Porto seamount (core MD95-2040) and the Sines coast (MD95-2042 in gray; MD01-2444 in gray; MD01-2443 in black) over the last 420 ka. a) $\delta^{18}O$ of *G. bulloides* records of cores MD95-2040 [*de Abreu et al*., 2003; this study], MD95-2042 [*Cayre et al*., 1999; *Shackleton et al*., 2000] and MD01-2443 [*de Abreu et al*., 2005; *Martrat et al*., 2007]; b) alkenone-based mean annual sea surface temperature (SST) records for cores MD95-2040 [*Pailler and Bard*, 2002] and MD01-2444 and MD01-2443 [*Martrat et al*., 2007]; c) foraminifer assemblage based summer SST and d) % *N. pachyderma* (s) records of cores MD95-2040 [*de Abreu et al*., 2003; this study], MD95-2042 [*Cayre et al*., 1999; *Salgueiro et al*., 2010] and MD01-2443 [*de Abreu et al*., 2005; this study]; and e) and f) benthic $\delta^{18}O$ and $\delta^{13}C$ records of cores MD95-2040 [*de Abreu et al*., 2003; *Schönfeld et al*., 2003; this

718 study], MD95-2042 [*Shackleton et al*., 2000] and MD01-2443 [*de Abreu et al*., 2005; *Martrat et*
719 *al*., 2007]. Numbers mark Marine Isotope Stages and T II, T III and T IV the terminations,
720 respectively. H11 indicates Heinrich event 11. Gray bars highlight events discussed in the text.
721
722 **Figure 6.** Vertical gradients in the upper water column at site MD95-2040 during Marine Isotope
723 Stage (MIS) 2 [*Voelker et al.*, 2009] and 4 [*de Abreu et al*., 2003; this study]. a): $\delta^{18}O$ records of
724 surface to thermocline dwelling species *G. ruber* white (red, Grw); *G. bulloides* (black; Gb); *N.*
725 *pachyderma* (r) (cyan; Npr); and *N. pachyderma* (s) (magenta; Nps). b): $\delta^{18}O$ records of winter
726 mixed layer species *G. inflata* (dark blue; Gi) and deep dwellers *G. scitula* (green; Gsc), *G.*
727 *truncatulinoides* (r) (light orange; Gtr) and *G. truncatulinoides* (s) (dark orange; Gts; only MIS
728 4). The respective $\delta^{13}C$ values are shown in panels e) and f). % *N. pachyderma* (s) data is plotted
729 in panels c) and the difference between $\delta^{18}O$ of *G. inflata* and $\delta^{18}O$ *of G. bulloides* reflecting
730 seasonality in panels d). Blue bars and H1, 2a, 2b, 3, and 6 mark the respective Heinrich stadials.
731 GI indicates respective Greenland interstadial.
732
733 **Figure 7.** Vertical gradients in the upper water column at site MD95-2041 during MIS 2 [*Voelker*
734 *et al.*, 2009] and 4 [this study]. Panels and foraminifer species as in Fig. 6.
735
736 **Figure 8**. Vertical gradients in in the upper water column at site MD95-2040 during MIS 6 [*de*
737 *Abreu et al*., 2003; this study]. Panels and foraminifer species as in Fig. 6. Blue bars mark periods
738 with increased seasonality. Numbers refer to MIS substages and H 11 to Heinrich event 11.
739
740 **Figure 9**. Vertical gradients in the upper water column at site MD01-2443 during MIS 6 [this
741 study]. a): $\delta^{18}O$ records of *G. ruber* white (red, Grw); *G. bulloides* (black; Gb); and *N.*
742 *pachyderma* (r) (cyan; Npr). b): $\delta^{18}O$ record of deep dweller *G. truncatulinoides* (r) (orange; Gtr).
743 The respective $\delta^{13}C$ values are shown in panels d) and e). Panel c) shows the magnetic
744 susceptibility record with peaks (also marked by blue bars) indicating ice-rafting events.
745 Numbers refer to MIS substages and H 11 to Heinrich event 11.
746
747 **Figure 10**. Vertical gradients in the hydrography at the southwestern Iberian margin over the last
748 65 ka in comparison to the Greenland (GISP2; a; [*Grootes and Stuiver*, 1997]) and Antarctic
749 (EDML; i; [*EPICA Community Members*, 2006]) ice core records. b) and c): Uppermost water
750 column conditions as reflected in the *G. ruber* white $\delta^{18}O$ values of cores MD99-2339 (black;
751 [*Voelker et al*., 2009; this study]) and MD99-2336 (gray; [*Voelker et al*., 2009; this study]) and in
752 the *G. bulloides* $\delta^{18}O$ data of core MD95-2042 [*Cayre et al.*, 1999; *Shackleton et al.*, 2000]. d):
753 ENACW-level subsurface water conditions based on the $\delta^{18}O$ of *G. truncatulinoides* from cores
754 MD99-2339 (black; [*Voelker et al*., 2009; this study]) and MD99-2336 (gray; [*Voelker et al*.,
755 2009; this study]). e): Response in the lower MOW's flow strength (core MD99-2339; [*Voelker*
756 *et al.*, 2006]) to the millennial-scale variability. f) and g): Deep water temperature changes at
757 2465 m (MD01-2444; [*Skinner and Elderfield*, 2007]) and at 3146 m (MD99-2334K; [*Skinner et*
758 *al.*, 2003]). h): Benthic $\delta^{18}O$ record of core MD95-2042 [*Shackleton et al.*, 2000]. GI, H and AIM
759 refer to Greenland interstadials, Heinrich stadials and Antarctic Isotope Maxima, respectively.
760 Depth ranges on the right refer to the living depths of the respective planktic foraminifer (a to c;
761 [*Voelker et al*., 2009]) or to the depth of the respective core site(s).
762
763 **Figure 11**. Vertical gradients in water column ventilation at the southwestern Iberian margin over
764 the last 65 ka in comparison to the Greenland (GISP2; a; [*Grootes and Stuiver*, 1997]) ice core
765 record. b) and c): Uppermost water column conditions as reflected in the *G. ruber* white $\delta^{13}C$

values of cores MD99-2339 (black; [*Voelker et al*., 2009; this study]) and MD99-2336 (gray; [*Voelker et al*., 2009; this study]) and in the *G. bulloides* $\delta^{13}C$ data of core MD95-2042 [*Cayre et al.*, 1999; *Shackleton et al.*, 2000]. d): ENACW-level subsurface water conditions based on the $\delta^{13}C$ of *G. truncatulinoides* from cores MD99-2339 (black; [*Voelker et al*., 2009; this study]) and MD99-2336 (gray; [*Voelker et al*., 2009; this study]). e): Ventilation changes in the lower MOW level (core MD99-2339; [*Voelker et al.*, 2006]). f): Benthic $\delta^{13}C$ data of cores MD95-2040 (black; [*de Abreu et al.*, 2003; *Schönfeld et al.*, 2003; this study]) and MD01-2444 (gray; [*Skinner and Elderfield*, 2007]). g): Benthic $\delta^{13}C$ records of cores MD95-2042 (black; [*Shackleton et al.*, 2000]) and MD99-2334K (gray; [*Skinner and Shackleton*, 2004]). h) Benthic $\delta^{13}C$ record of core MD03-2698 [*Lebreiro et al.*, 2009]. Nomenclature and depth ranges as in Fig. 10.

References

Alvarez, M., F. F. Perez, H. Bryden, and A. F. Rios (2004), Physical and biogeochemical transports structure in the North Atlantic subpolar gyre, *J. Geophys. Res., 109*(C3), C03027, doi: 10.1029/2003jc002015.

Alvarez-Salgado, X. A., et al. (2003), The Portugal coastal counter current off NW Spain: new insights on its biogeochemical variability, *Prog. Oceanogr.*, *56*(2), 281-321.

Ambar, I., and M. R. Howe (1979), Observations of the Mediterranean Outflow: 1. Mixing in the Mediterranean Outflow, *Deep Sea Res.*, *26*(5), 535-554.

Baas, J. H., J. Schönfeld, and R. Zahn (1998), Mid-depth oxygen drawdown during Heinrich events: evidence from benthic foraminiferal community structure, trace-fossil tiering, and benthic $\delta^{13}C$ at the Portuguese Margin, *Mar. Geol.*, *152*, 25-55.

Baas, J. H., J. Mienert, F. Abrantes, and M. A. Prins (1997), Late Quaternary sedimentation on the Portuguese continental margin: climate-related processes and products, *Palaeogeogr. Palaeoclimat. Palaeoecol.*, *130*, 1-23.

Bard, E., F. Rostek, J.-L. Turon, and S. Gendreau (2000), Hydrological Impact of Heinrich Events in the Subtropical Northeast Atlantic, *Science*, *289*, 1321-1324.

Bassetti, M. A., P. Carbonel, F. J. Sierro, M. Perez-Folgado, G. Jouit, and S. Berne (2010), Response of ostracods to abrupt climate changes in the Western Mediterranean (Gulf of Lions) during the last 30 kyr, *Mar. Micropaleontol.*, *77*(1-2), 1-14.

Bassinot, F., and L. Labeyrie (1996), IMAGES MD 101 A coring cruise of the R/V Marion Dufresne in the North Atlantic and Norwegian Sea. *Rep.*, 217 pp, Institut Francais pour la Recherche et la Technologie Polaires, Plouzane.

Bemis, B. E., H. J. Spero, D. W. Lea, and J. Bijma (2000), Temperature influence on the carbon isotopic composition of *Globigerina bulloides* and *Orbulina universa* (planktonic foraminifera), *Mar. Micropaleontol.*, *38*(3-4), 213-228.

Brambilla, E., L. D. Talley, and P. E. Robbins (2008), Subpolar Mode Water in the northeastern Atlantic: 2. Origin and transformation, *J. Geophys. Res., 113,* C04026, doi: 10.1029/2006JC004063.

Cabeçadas, G., M. J. Brogueira, and C. Gonçalves (2003), Intermediate water masses off south-southwest Portugal: Chemical tracers, *J. Mar. Res.*, *61*(4), 539-552.

Cacho, I., J. O. Grimalt, F. J. Sierro, N. Shackleton, and M. Canals (2000), Evidence for enhanced Mediterranean thermohaline circulation during rapid climatic coolings, *Earth Planet. Sci. Lett.*, *183*, 417-429.

812 Cayre, O., Y. Lancelot, E. Vincent, and M. A. Hall (1999), Paleoceanographic reconstructions
813 from planktonic foraminifera off the Iberian margin: temperature, salinity, and Heinrich
814 events, *Paleoceanography*, *14*, 384–396.
815 Colmenero-Hidalgo, E., J.-A. Flores, F. J. Sierro, M. A. Barcena, L. Loewemark, J. Schönfeld,
816 and J. O. Grimalt (2004), Ocean surface water response to short-term climate changes revealed
817 by coccolithophores from the Gulf of Cadiz (NE Atlantic) and Alboran Sea (W
818 Mediterranean), *Palaeogeogr. Palaeoclimat. Palaeoecol.*, *205*(3-4), 317-336.
819 Curry, W. B., and D. W. Oppo (2005), Glacial water mass geometry and the distribution of $\delta^{13}C$
820 of ΣCO_2 in the western Atlantic Ocean, *Paleoceanography, 20*(1), PA1017, doi:
821 10.1029/2004PA001021.
822 de Abreu, L., N. J. Shackleton, J. Schönfeld, M. Hall, and M. Chapman (2003), Millennial-scale
823 oceanic climate variability off the Western Iberian margin during the last two glacial periods,
824 *Mar. Geol.*, *196*(1-2), 1-20.
825 de Abreu, L., F. F. Abrantes, N. J. Shackleton, P. C. Tzedakis, J. F. McManus, D. W. Oppo, and
826 M. A. Hall (2005), Ocean climate variability in the eastern North Atlantic during interglacial
827 marine isotope stage 11: A partial analogue to the Holocene?, *Paleoceanography, 20*(3),
828 PA3009, doi: 10.1029/2004PA001091.
829 de Vargas, C., S. Renaud, H. Hilbrecht, and J. Pawlowski (2001), Pleistocene adaptive radiation
830 in Globorotalia truncatulinoides: genetic, morphologic, and environmental evidence,
831 *Paleobiol.*, *27*(1), 104-125.
832 Dickson, R. R., J. Meincke, S.-A. Malmberg, and A. J. Lee (1988), The "great salinity anomaly"
833 in the northern North Atlantic 1968 –1982, *Prog. Oceanogr.*, *20*, 103– 151.
834 EPICA Community Members (2006), One-to-one coupling of glacial climate variability in
835 Greenland and Antarctica, *Nature*, *444*, 195-198.
836 Eynaud, F., et al. (2009), Position of the Polar Front along the western Iberian margin during key
837 cold episodes of the last 45 ka, *Geochem. Geophys. Geosyst., 10*(7), Q07U05, doi:
838 10.1029/2009GC002398.
839 Fiuza, A. F. G., M. Hamann, I. Ambar, G. D. del Rio, N. Gonzalez, and J. M. Cabanas (1998),
840 Water masses and their circulation off western Iberia during May 1993, *Deep Sea Res., Part I*,
841 *45*(7), 1127-1160.
842 Fiúza, A. F. G. (1984), Hidrologia e Dinamica das Aguas Costeiras de Portugal, Doctorate thesis,
843 294 pp, Universidade de Lisboa, Lisbon.
844 Fletcher, W. J., et al. (2010), Millennial-scale variability during the last glacial in vegetation
845 records from Europe, *Quat. Sci. Rev.*, *29*(21-22), 2839-2864.
846 Frouin, R., A. F. G. Fiuza, I. Ambar, and T. J. Boyd (1990), Observations of a Poleward Surface
847 Current Off the Coasts of Portugal and Spain during Winter, *J. Geophys. Res.*, *95*(C1), 679-
848 691.
849 Ganssen, G. M., and D. Kroon (2000), The isotopic signature of planktonic foraminifera from NE
850 Atlantic surface sediments: implications for the reconstruction of past oceanic conditions, *J.*
851 *Geol. Soc. London*, *157*, 693-699.
852 Garcia-Lafuente, J., J. Delgado, F. Criado-Aldeanueva, M. Bruno, J. del Rio, and J. Miguel
853 Vargas (2006), Water mass circulation on the continental shelf of the Gulf of Cadiz, *Deep Sea*
854 *Res., Part II*, *53*(11-13), 1182-1197.
855 Grootes, P. M., and M. Stuiver (1997), $^{18}O/^{16}O$ variability in Greenland snow and ice with 10^{-3}
856 to 10^{5} year time resolution, *J. Geophys. Res.*, *102*(C12), 26,455–426,470.
857 Haynes, R., and E. D. Barton (1990), A Poleward Flow Along the Atlantic Coast of the Iberian
858 Peninsula, *J. Geophys. Res.*, *95*(C7), 11425-11441.

859 Haynes, R., E. D. Barton, and I. Pilling (1993), Development, Persistence, and Variability of
860 Upwelling Filaments Off the Atlantic Coast of the Iberian Peninsula, *J. Geophy. Res.*,
861 *98*(C12), 22681-22692.
862 Hemming, S. R. (2004), Heinrich events: Massive late Pleistocene detritus layers of the North
863 Atlantic and their global climate imprint, *Rev. Geophys., 42* (1), RG1005, doi:
864 10.1029/2003RG000128
865 Hodell, D. A., J. E. T. Channell, J. H. Curtis, O. E. Romero, and U. Röhl (2008), Onset of
866 'Hudson Strait' Heinrich Events in the Eastern North Atlantic at the end of the Middle
867 Pleistocene Transition (~640 ka)?, *Paleoceanography, 23*, PA4218, doi:
868 10.1029/2008PA001591.
869 Hughen, K., S. Lehman, J. Southon, J. Overpeck, O. Marchal, C. Herring, and J. Turnbull (2004),
870 ^{14}C Activity and Global Carbon Cycle Changes over the Past 50,000 Years, *Science*, *303*, 202-
871 207.
872 Incarbona, A., B. Martrat, E. Di Stefano, J. O. Grimalt, N. Pelosi, B. Patti, and G. Tranchida
873 (2010), Primary productivity variability on the Atlantic Iberian Margin over the last 70,000
874 years: Evidence from coccolithophores and fossil organic compounds, *Paleoceanography*,
875 *25*(2), PA2218, doi: 10.1029/2008pa001709.
876 Jia, Y. (2000), Formation of an Azores Current due to Mediterranean Overflow in a modeling
877 study of the North Atlantic, *J. Phys. Oceanogr.*, *30*, 2342-2358.
878 Johnson, J., and I. Stevens (2000), A fine resolution model of the eastern North Atlantic between
879 the Azores, the Canary Islands and the Gibraltar Strait, *Deep Sea Res., Part I*, *47*(5), 875-899.
880 Kjellström, E., J. Brandefelt, J. O. Näslund, B. Smith, G. Strandberg, A. H. L. Voelker, and B.
881 Wohlfarth (2010), Simulated climate conditions in Europe during the Marine Isotope Stage 3
882 stadial, *Boreas*, *39*(2), 436-456.
883 Kuhnt, T., G. Schmiedl, W. Ehrmann, Y. Hamann, and N. Andersen (2008), Stable isotopic
884 composition of Holocene benthic foraminifers from the Eastern Mediterranean Sea: Past
885 changes in productivity and deep water oxygenation, *Palaeogeogr. Palaeoclimatol.*
886 *Palaeoecol.*, *268*(1-2), 106-115.
887 Labeyrie, L., E. Jansen, and E. Cortijo (Eds.) (2003), *MD 114 / IMAGES V, á bord du Marion*
888 *Dufresne, Fort de France, 11 juin 1999 - Marseille, 20 Septembre 1999*, 1-380 and 381-849
889 pp., Institut Polaire Francais Paul-Emile Victor.
890 Lebreiro, S. M., A. H. L. Voelker, A. Vizcaino, F. G. Abrantes, U. Alt-Epping, S. Jung, N.
891 Thouveny, and E. Gracia (2009), Sediment instability on the Portuguese continental margin
892 under abrupt glacial climate changes (last 60 kyr), *Quat. Sci. Rev.*, *28*(27-28), 3211-3223.
893 Lisiecki, L. E., and M. Raymo (2005), A Pliocene-Pleistocene stack of 57 globally distributed
894 benthic δ^{18}O records, *Paleoceanography, 20*, PA1003, doi: 10.1029/2004PA001071.
895 Llave, E., J. Schönfeld, F. J. Hernandez-Molina, T. Mulder, L. Somoza, V. Diaz del Rio, and I.
896 Sanchez-Almazo (2006), High-resolution stratigraphy of the Mediterranean outflow contourite
897 system in the Gulf of Cadiz during the late Pleistocene: The impact of Heinrich events, *Mar.*
898 *Geol.*, *227*(3-4), 241-262.
899 Lowe, J., W. Z. Hoek, and INTIMATE group (2001), Inter-regional correlation of palaeoclimatic
900 records for the Last Glacial-Interglacial Transition: a protocol for improved precision
901 recommended by the INTIMATE project group, *Quat. Sci. Rev.*, *20*(11), 1175-1187.
902 Lowe, J. J., S. O. Rasmussen, S. Björck, W. Z. Hoek, J. P. Steffensen, M. J. C. Walker, and Z. C.
903 Yu (2008), Synchronisation of palaeoenvironmental events in the North Atlantic region during
904 the Last Termination: a revised protocol recommended by the INTIMATE group, *Quat. Sci.*
905 *Rev.*, *27*(1-2), 6-17.

906 Mackensen, A., H.-W. Hubberten, T. Bickert, G. Fischer, and D. K. Fütterer (1993), The $\delta^{13}C$ in
907 benthic foraminiferal tests of *Fontbotia wuellerstorfi* (Schwager) relative to the $\delta^{13}C$ of
908 dissolved inorganic carbon in Southern Ocean deep water: Implications for glacial ocean
909 circulation models, *Paleoceanography*, *8*(5), 587–610.
910 Margari, V., L. C. Skinner, P. C. Tzedakis, A. Ganopolski, M. Vautravers, and N. J. Shackleton
911 (2010), The nature of millennial-scale climate variability during the past two glacial periods,
912 *Nature Geosci.*, *3*(2), 127-131.
913 Martrat, B., J. O. Grimalt, N. J. Shackleton, L. de Abreu, M. A. Hutterli, and T. F. Stocker
914 (2007), Four Climate Cycles of Recurring Deep and Surface Water Destabilizations on the
915 Iberian Margin, *Science*, *317*, 502-507.
916 McCartney, M. S., and L. D. Talley (1982), The Sub-Polar Mode Water of the North-Atlantic
917 Ocean, *J. Phys. Oceanogr.*, *12*(11), 1169-1188.
918 Moreno, E., N. Thouveny, D. Delanghe, I. N. McCave, and N. J. Shackleton (2002), Climatic and
919 oceanographic changes in the Northeast Atlantic reflected by magnetic properties of sediments
920 deposited on the Portuguese Margin during the last 340 ka, *Earth Planet. Sci. Lett.*, *202*(2),
921 465-480.
922 Naughton, F., M. F. Sanchez Goni, S. Desprat, J. L. Turon, J. Duprat, B. Malaize, C. Joli, E.
923 Cortijo, T. Drago, and M. C. Freitas (2007), Present-day and past (last 25 000 years) marine
924 pollen signal off western Iberia, *Mar. Micropaleontol.*, *62*(2), 91-114.
925 Naughton, F., et al. (2009), Wet to dry climatic trend in north-western Iberia within Heinrich
926 events, *Earth Planet. Sci. Lett.*, *284*(3-4), 329-342.
927 Navarro, G., and J. Ruiz (2006), Spatial and temporal variability of phytoplankton in the Gulf of
928 Cadiz through remote sensing images, *Deep Sea Res., Part II*, *53*(11-13), 1241-1260.
929 NGRIP members (2004), High-resolution record of Northern Hemisphere climate extending into
930 the last interglacial period, *Nature*, *431*(7005), 147-151.
931 Oezgoekmen, T. M., E. P. Chassignet, and C. G. H. Rooth (2001), On the connection between the
932 Mediterranean Outflow and the Azores Current, *J. Phys. Oceanogr.*, *31*, 461-480.
933 Pahnke, K., S. L. Goldstein, and S. R. Hemming (2008), Abrupt changes in Antarctic
934 Intermediate Water circulation over the past 25,000 years, *Nature Geosci.*, *1*(12), 870-874.
935 Pailler, D., and E. Bard (2002), High frequency palaeoceanographic changes during the past
936 140000 yr recorded by the organic matter in sediments of the Iberian Margin, *Palaeogeogr.*
937 *Palaeoclimat. Palaeoecol.*, *181*(4), 431-452.
938 Peliz, A., J. Dubert, P. Marchesiello, and A. Teles-Machado (2007), Surface circulation in the
939 Gulf of Cadiz: Model and mean flow structure, *J. Geophys. Res., 112*(C11015), doi:
940 10.1029/2007JC004159.
941 Peliz, A., J. Dubert, A. M. P. Santos, P. B. Oliveira, and B. Le Cann (2005), Winter upper ocean
942 circulation in the Western Iberian Basin – Fronts, Eddies and Poleward Flows: an overview,
943 *Deep Sea Res., Part I*, *52*(4), 621-646.
944 Penduff, T., A. C. de Verdiere, and B. Barnier (2001), General circulation and intergyre
945 dynamics in the eastern North Atlantic from a regional primitive equation model, *J. Geophys.*
946 *Res.*, *106*(C10), 22313-22329.
947 Perez, F. F., C. G. Castro, X. A. Alvarez-Salgado, and A. F. Rios (2001), Coupling between the
948 Iberian basin - scale circulation and the Portugal boundary current system: a chemical study,
949 *Deep-Sea Res., Part I*, *48*(6), 1519-1533.
950 Pflaumann, U., J. Duprat, C. Pujol, and L. D. Labeyrie (1996), SIMMAX: A modern analog
951 technique to deduce Atlantic sea surface temperatures from planktonic foraminifera in deep-
952 sea sediments, *Paleoceanography*, *11*(1), 15-36.

953 Pflaumann, U., et al. (2003), Glacial North Atlantic: Sea-surface conditions reconstructed by
954 GLAMAP 2000, *Paleoceanography, 18*(3), 1065, doi: 10.1029/2002PA000774.
955 Pingree, R. D., C. Garcia-Soto, and B. Sinha (1999), Position and structure of the Subtropical
956 /Azores Front region from combined Lagrangian and remote sensing (IR/altimeter/SeaWiFS)
957 measurements, *J Mar. Biol. Assoc. United Kingdom*, *79*(5), 769-792.
958 Rashid, H., and E. A. Boyle (2007), Mixed-Layer Deepening During Heinrich Events: A Multi-
959 Planktonic Foraminiferal $\delta^{18}O$ Approach, *Science*, *318*(5849), 439-441.
960 Relvas, P., and E. D. Barton (2002), Mesoscale patterns in the Cape São Vicente (Iberian
961 Peninsula) upwelling region, *J. Geophys. Res.*, *107*(C10), 28-21-28-23.
962 Richardson, P. L., A. S. Bower, and W. Zenk (2000), A census of Meddies tracked by floats,
963 *Progr. Oceanogr.*, *45*, 209-250.
964 Rios, A. F., F. F. Perez, and F. Fraga (1992), Water Masses in the Upper and Middle North-
965 Atlantic Ocean East of the Azores, *Deep Sea Res., Part A*, *39*(3-4A), 645-658.
966 Rogerson, M., E. J. Rohling, P. P. E. Weaver, and J. W. Murray (2004), The Azores Front since
967 the Last Glacial Maximum, *Earth Planet. Sci. Lett.*, *222*(3-4), 779-789.
968 Rogerson, M., E. J. Rohling, P. P. E. Weaver, and J. W. Murray (2005), Glacial to interglacial
969 changes in the settling depth of the Mediterranean Outflow plume, *Paleoceanography, 20*(3),
970 PA3007, doi: 10.1029/2004PA001106.
971 Roucoux, K. H., L. de Abreu, N. J. Shackleton, and P. C. Tzedakis (2005), The response of NW
972 Iberian vegetation to North Atlantic climate oscillations during the last 65 kyr, *Quat. Sci. Rev.*,
973 *24*(14-15), 1637-1653.
974 Ruddiman, W. F. (1977), Late Quaternary deposition of ice-rafted sand in the subpolar North
975 Atlantic (lat 40º to 65ºN), *Geol. Soc. Am. Bull.*, *88*, 1813-1827.
976 Salgueiro, E., A. H. L. Voelker, L. de Abreu, F. Abrantes, H. Meggers, and G. Wefer (2010),
977 Temperature and productivity changes off the western Iberian margin during the last 150 ky,
978 *Quat. Sci. Rev.*, *29*(5-6), 680-695.
979 Sanchez-Goñi, M. F., and S. P. Harrison (2010), Millennial-scale climate variability and
980 vegetation changes during the Last Glacial: Concepts and terminology, *Quat. Sci. Rev.*, *29*(21-
981 22), 2823-2827.
982 Sánchez-Goñi, M. F., A. Landais, W. J. Fletcher, F. Naughton, S. Desprat, and J. Duprat (2008),
983 Contrasting impacts of Dansgaard-Oeschger events over a western European latitudinal
984 transect modulated by orbital parameters, *Quat. Sci. Rev.*, *27*(11-12), 1136-1151.
985 Sanchez, R. F., and P. Relvas (2003), Spring-summer climatological circulation in the upper
986 layer in the region of Cape St. Vincent, Southwest Portugal, *ICES J. Mar. Sci.*, *60*(6), 1232-
987 1250.
988 Sarnthein, M., et al. (2001), Fundamental modes and abrupt changes in North Atlantic circulation
989 and climate over the last 60 ky – Numerical modelling and reconstruction, in *The Northern*
990 *North Atlantic: A changing environment*, edited by P. Schäfer, W. Ritzrau, M. Schlüter and J.
991 Thiede, pp. 365–410, Springer Verlag, Heidelberg.
992 Saunders, P. M. (1987), Flow through Discovery Gap, *J. Phys. Oceanogr., 17*, 631-643.
993 Schlitzer, R. (2000), Electronic Atlas of WOCE Hydrographic and Tracer Data Now Available,
994 *Eos Trans. AGU*, *81*(5), 45.
995 Schmiedl, G., T. Kuhnt, W. Ehrmann, K.-C. Emeis, Y. Hamann, U. Kotthoff, P. Dulski, and J.
996 Pross (in press), Climatic forcing of eastern Mediterranean deep-water formation and benthic
997 ecosystems during the past 22 000 years, *Quat. Sci. Rev.* doi:
998 10.1016/j.quascirev.2010.07.002.

Schönfeld, J., and R. Zahn (2000), Late Glacial to Holocene history of the Meditarranean Outflow. Evidence from benthic Foraminiferal assemblages and stable isotopes at the Portuguese margin, *Palaeogeogr. Palaeoclimat. Palaeoecol.*, *159*, 85-111.

Schönfeld, J., R. Zahn, and L. de Abreu (2003), Surface and deep water response to rapid climate changes at the Western Iberian margin, *Global Planet. Change*, *36*(4), 237-264

Serra, N., and I. Ambar (2002), Eddy generation in the Mediterranean undercurrent, *Deep Sea Res., Part II*, *49*(19), 4225-4243.

Shackleton, N. J., M. A. Hall, and E. Vincent (2000), Phase relationships between millennial-scale events 64,000-24,000 years ago, *Paleoceanography*, *15*(6), 565-569.

Sierro, F. J., et al. (2005), Impact of iceberg melting on Mediterranean thermohaline circulation during Heinrich events, *Paleoceanography, 20*(2), PA2019, doi: 10.1029/2004PA001051.

Skinner, L. C., and N. J. Shackleton (2004), Rapid transient changes in northeast Atlantic deep water ventilation age across Termination I, *Paleoceanography 19* (2), PA2005, doi: 10.1029/2003PA000983

Skinner, L. C., and H. Elderfield (2007), Rapid fluctuations in the deep North Atlantic heat budget during the last glacial period, *Paleoceanography, 22*(1), PA1205, doi: 10.1029/2006PA001338.

Skinner, L. C., N. J. Shackleton, and H. Elderfield (2003), Millennial-scale variability of deep-water temperature and $\delta^{18}O_{dw}$ indicating deep-water source variations in the Northeast Atlantic, 0-34 cal. ka BP, *Geochem. Geophys. Geosyst., 4*(12), 1098, doi: 10.1029/2003GC000585.

Sousa, F. M., and A. Bricaud (1992), Satellite-Derived Phytoplankton Pigment Structures in the Portuguese Upwelling Area, *J. Geophys. Res.*, *97*(C7), 11343-11356.

Stein, R., J. Hefter, J. Grützner, A. Voelker, and B. D. A. Naafs (2009), Variability of surface-water characteristics and Heinrich-like Events in the Pleistocene mid-latitude North Atlantic Ocean: Biomarker and XRD records from IODP Site U1313 (MIS 16 – 9), *Paleoceanography, 24*, PA2203, doi: 10.1029/2008PA001639.

Thomson, J., S. Nixon, C. P. Summerhayes, E. J. Rohling, J. Schönfeld, R. Zahn, P. Grootes, F. Abrantes, L. Gaspar, and S. Vaqueiro (2000), Enhanced productivity on the Iberian margin during glacial/interglacial transitions revealed by barium and diatoms, *J. Geol. Soc. London*, *157*(3), 667-677.

Thouveny, N., J. Carcaillet, E. Moreno, G. Leduc, and D. Nerini (2004), Geomagnetic moment variation and paleomagnetic excursions since 400 kyr BP: a stacked record from sedimentary sequences of the Portuguese margin, *Earth Planet. Sci. Lett.*, *219*, 377-396.

Toucanne, S., T. Mulder, J. Schoenfeld, V. Hanquiez, E. Gonthier, J. Duprat, M. Cremer, and S. Zaragosi (2007), Contourites of the Gulf of Cadiz: A high-resolution record of the paleocirculation of the Mediterranean outflow water during the last 50,000 years, *Palaeogeogr. Palaeoclimatol. Palaeoecol.*, *246*(2-4), 354-366.

Toucanne, S., et al. (2009), Timing of massive 'Fleuve Manche' discharges over the last 350 kyr: insights into the European ice-sheet oscillations and the European drainage network from MIS 10 to 2, *Quat. Sci. Rev.*, *28*(13-14), 1238-1256.

Tzedakis, P. C., H. Pälike, K. H. Roucoux, and L. de Abreu (2009), Atmospheric methane, southern European vegetation and low-mid latitude links on orbital and millennial timescales, *Earth Planet. Sci. Lett.*, *277*(3-4), 307-317.

van Aken, H. M. (2000), The hydrography of the mid-latitude Northeast Atlantic Ocean – Part I: The deep water masses, *Deep Sea Res., Part I*, *47*, 757-788.

van Aken, H. M. (2001), The hydrography of the mid-latitude Northeast Atlantic Ocean – Part III: the subducted thermocline water mass, *Deep Sea Res., Part I*, *48*(1), 237-267.

1047 Vargas, J. M., J. Garcia-Lafuente, J. Delgado, and F. Criado (2003), Seasonal and wind-induced
1048 variability of Sea Surface Temperature patterns in the Gulf of Cadiz, *J. Mar. Systems*, *38*(3-4),
1049 205-219.
1050 Vautravers, M. J., and N. J. Shackleton (2006), Centennial-scale surface hydrology off Portugal
1051 during marine isotope stage 3: Insights from planktonic foraminiferal fauna variability,
1052 *Paleoceanography, 21*(3), PA3004, doi: 10.1029/2005PA001144.
1053 Voelker, A. H. L., L. de Abreu, J. Schönfeld, H. Erlenkeuser, and F. Abrantes (2009),
1054 Hydrographic Conditions Along the Western Iberian Margin During Marine Isotope Stage 2,
1055 *Geochem. Geophys. Geosyst., 10,* Q12U08, doi: 10.1029/2009GC002605.
1056 Voelker, A. H. L., S. M. Lebreiro, J. Schönfeld, I. Cacho, H. Erlenkeuser, and F. Abrantes
1057 (2006), Mediterranean outflow strengthening during northern hemisphere coolings: A salt
1058 source for the glacial Atlantic?, *Earth Planet. Sci. Lett.*, *245*(1-2), 39-55.
1059 Willamowski, C., and R. Zahn (2000), Upper ocean circulation in the glacial North Atlantic from
1060 benthic foraminiferal isotope and trace element fingerprinting, *Paleoceanography*, *15*, 515–
1061 527.
1062 Zahn, R., J. Schönfeld, H. Kudrass, M. Park, H. Erlenkeuser, and P. Grootes (1997),
1063 Thermohaline instability in the North Atlantic during meltwater events: Stable isotope and ice-
1064 rafted detritus records from core SO75-26KL, Portuguese margin, *Paleoceanography*, *12*(5),
1065 696-710.
1066

Table 1: List of core sites and references for data and age models

Core number	Longitude	Latitude	Water depth (m)	Data sources	Age model
SU92-03	43.20°N	10.11°W	3005	*Salgueiro et al*. [2010]	*Salgueiro et al*. [2010]: GISP2
MD99-2331	42.15°N	9.68°W	2110	*Sánchez-Goñi et al*. [2008]	*Sánchez-Goñi et al*. [2008]: NGRIP tuned
MD95-2040	40.58°N	9.86°W	2465	*de Abreu et al*. [2003]; *Schönfeld et al*. [2003]; *Pailler and Bard* [2002]; this study	*Salgueiro et al*. [2010] for MIS 1-3, MIS 4-5 tuned to MD95-2042; MIS 6: *Margari et al*. [2010]; ≥MIS 7: tuned to LR04
MD03-2698	38.24°N	10.39°W	4602	*Lebreiro et al*. [2010]	*Lebreiro et al*. [2010]
MD95-2041	37.83°N	9.52°W	1123	*Voelker et al*. [2009]; this study	*Voelker et al*. [2009] and tuning to MD95-2042 for >30 ka
MD95-2042	37.80°N	10.17°W	3146	*Cayre et al*. [1999]; *Shackleton et al*. [2000]; *Sánchez-Goñi et al*. [2008]; this study (SIMMAX SST)	*Shackleton et al*. [2000]: GISP2
MD99-2334K	37.80°N	10.17°W	3146	*Skinner et al*. [2003]	*Skinner et al*. [2003]: GISP2
MD01-2443	37.88°N	10.18°W	2941	*de Abreu et al*. [2005]; *Tzedakis et al*. [2004]; *Martrat et al*. [2007]; this study	*Tzedakis et al*. [2009]: tuned to EDC3
MD01-2444	37.57°N	10.13°W	2656	*Vautravers and Shackleton* [2006]; *Martrat et al*. [2007]; *Skinner and Elderfield* [2004; 2006; 2007]; this study (SIMMAX SST)	*Vautravers and Shackleton* [2006] modified to GISP2 ages for MIS 3 and *Martrat et al*. [2007]
MD99-2336	36.72°N	8.26°W	690	*Voelker et al*. [2009]; this study	*Voelker et al*. [2009] and tuning to MD95-2042 for MIS 4
MD99-2339	35.89°N	7.53°W	1170	*Voelker et al*. [2006, 2009]; this study	*Voelker et al*. [2006]

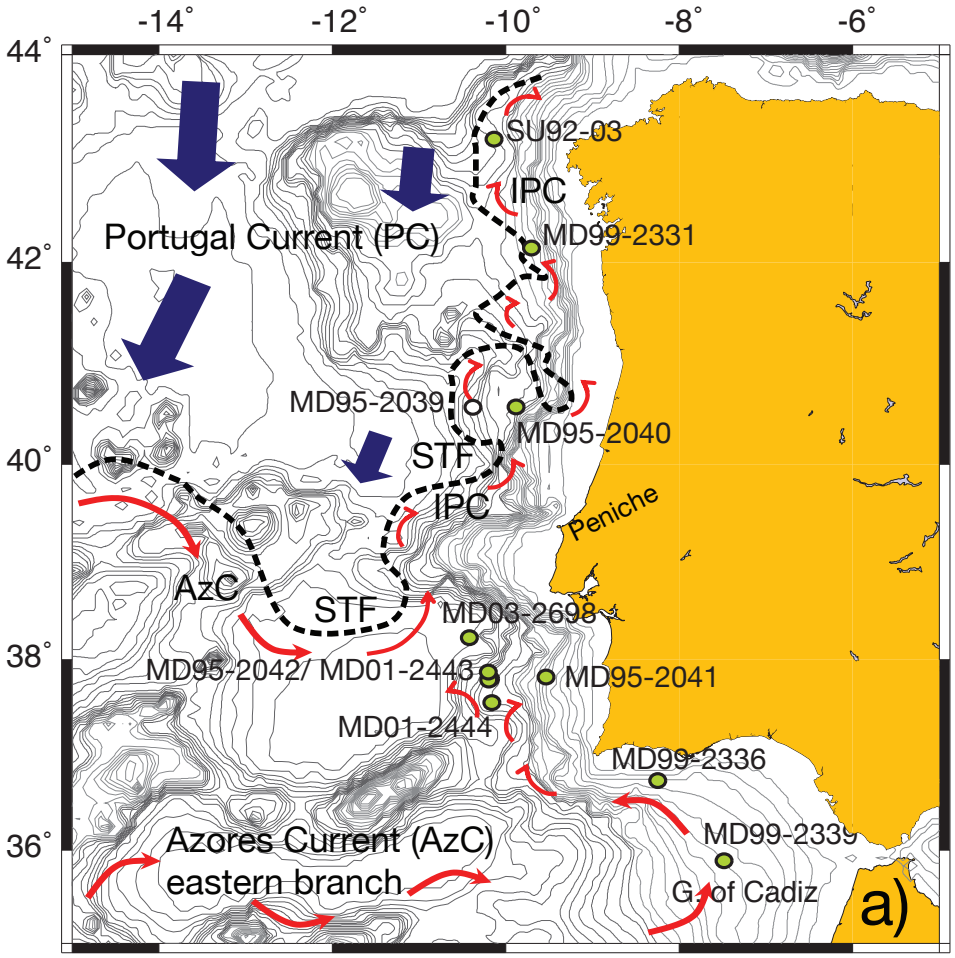

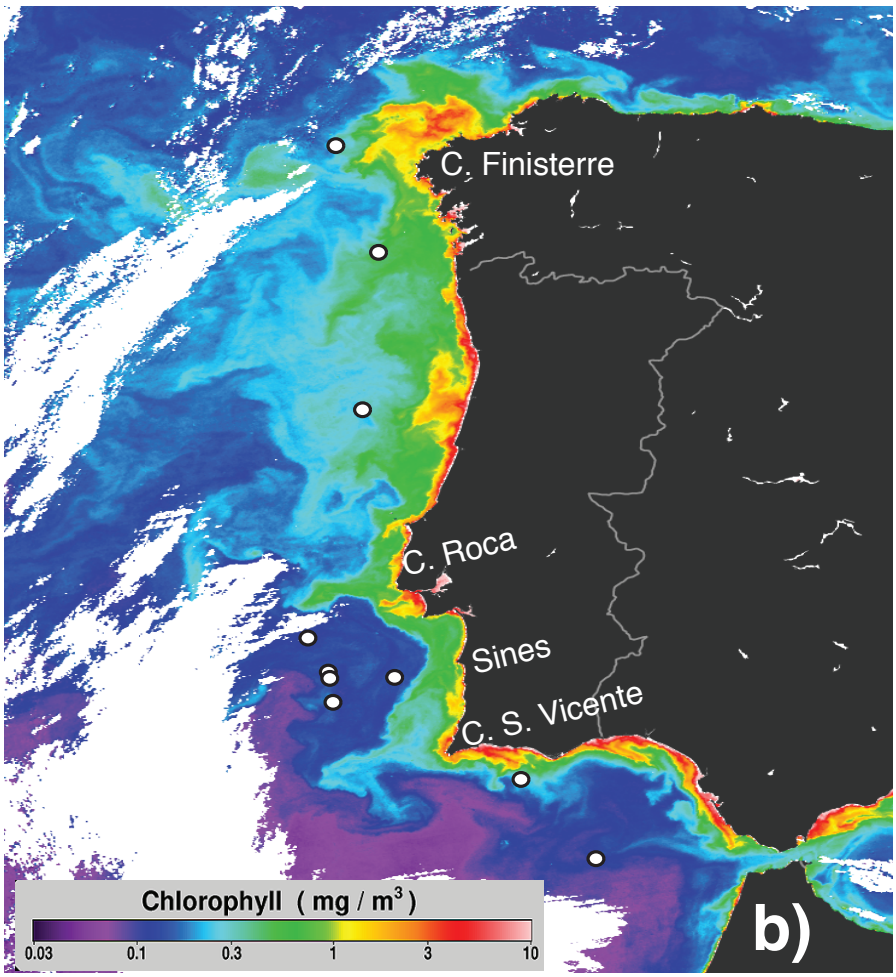

Voelker & de Abreu Figure 1

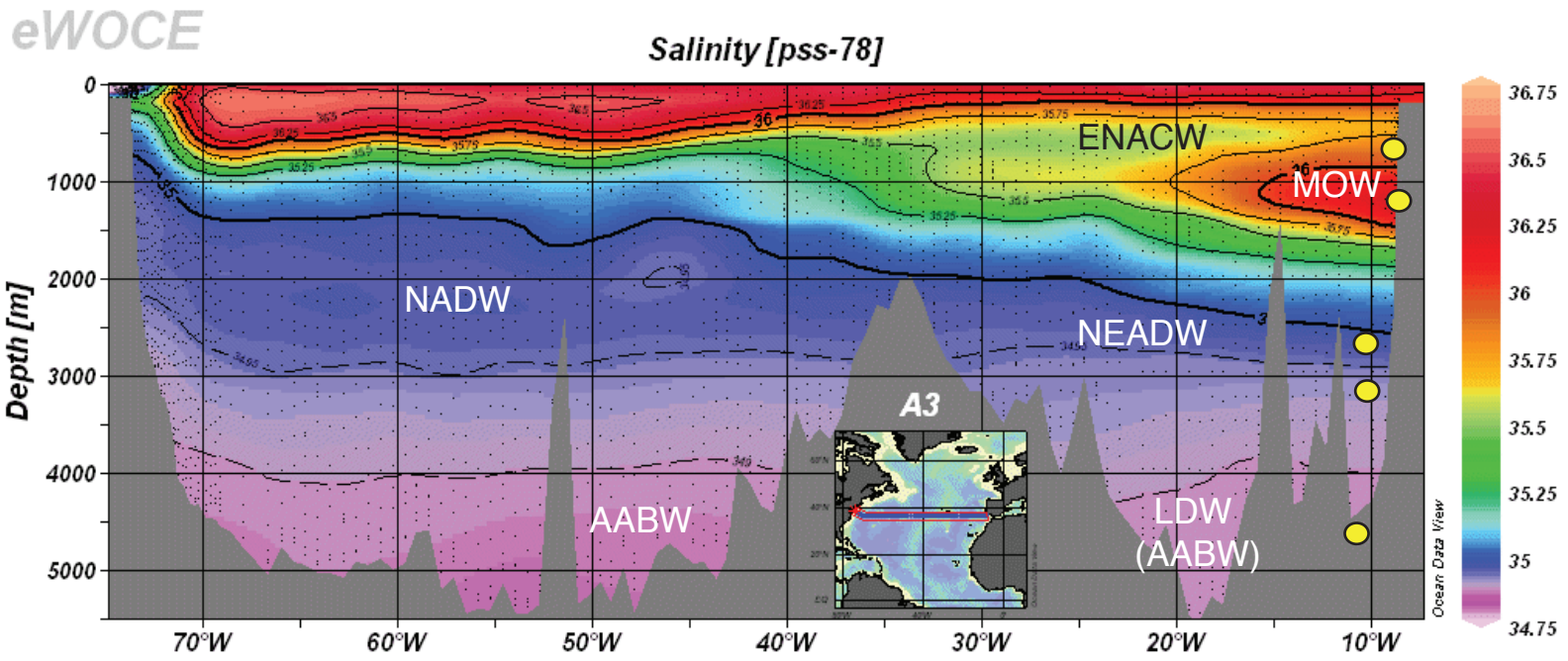
eWOCE
Salinity [pss-78]
Depth [m]
0
1000
2000
3000
4000
5000
70°W
60°W
50°W
40°W
30°W
20°W
10°W
ENACW
MOW
NADW
NEADW
AABW
LDW
(AABW)
A3
36.75
36.5
36.25
36
35.75
35.5
35.25
35
34.75
Ocean Data View

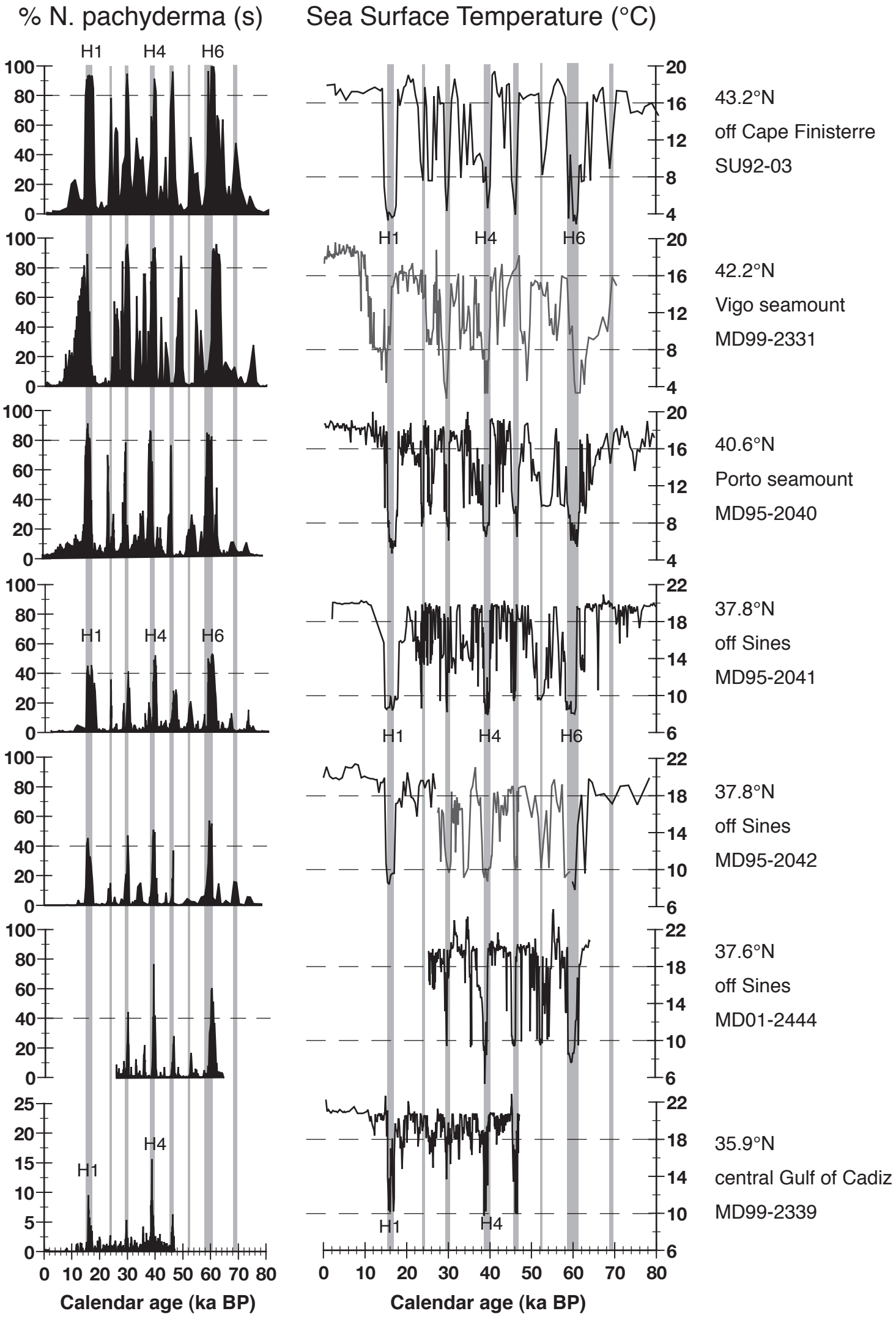
% N. pachyderma (s)
Sea Surface Temperature (°C)
H1
H4
H6
43.2°N
off Cape Finisterre
SU92-03
42.2°N
Vigo seamount
MD99-2331
40.6°N
Porto seamount
MD95-2040
37.8°N
off Sines
MD95-2041
37.8°N
off Sines
MD95-2042
37.6°N
off Sines
MD01-2444
35.9°N
central Gulf of Cadiz
MD99-2339
Calendar age (ka BP)
Calendar age (ka BP)

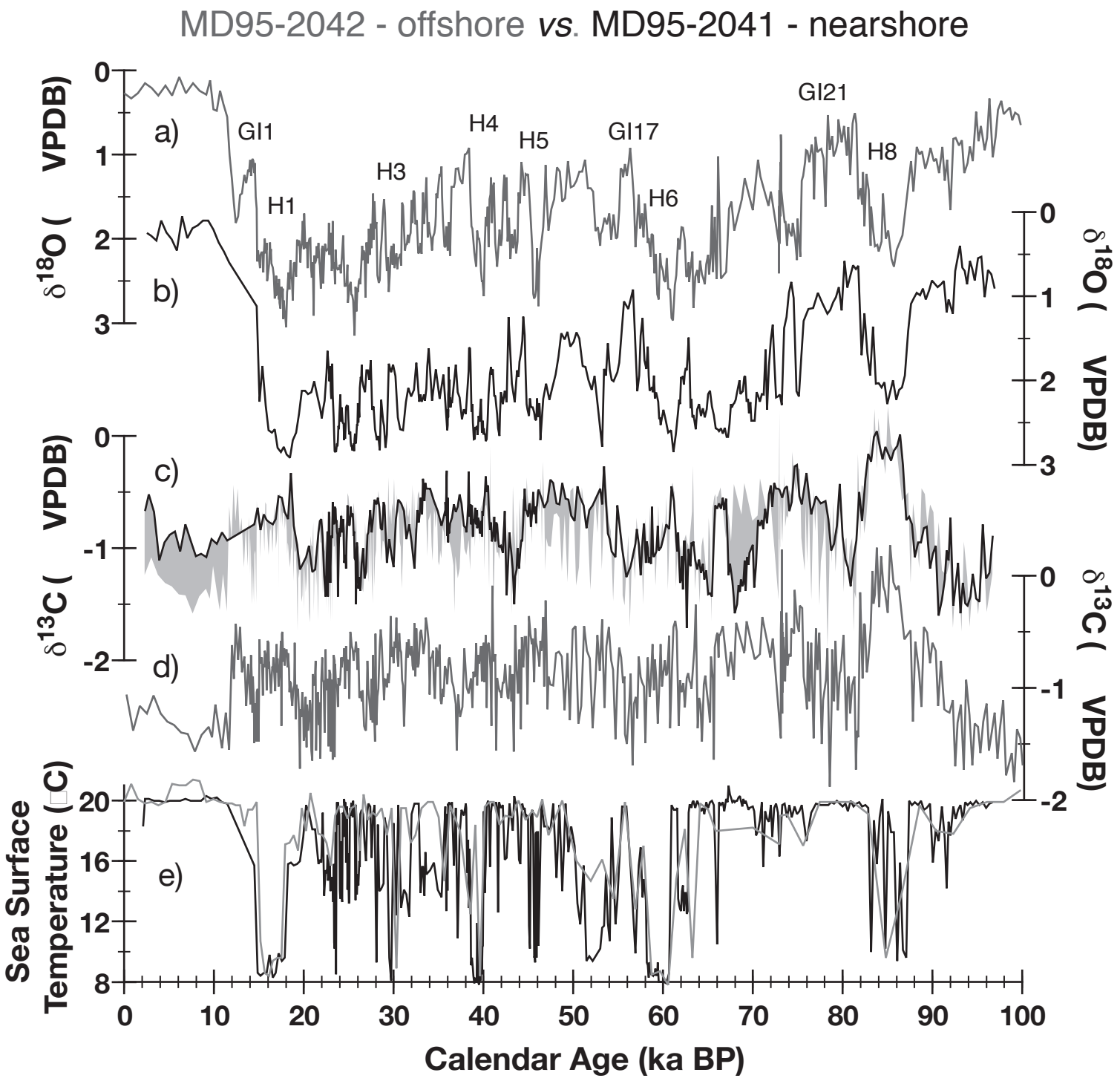

Voelker & de Abreu Figure 4

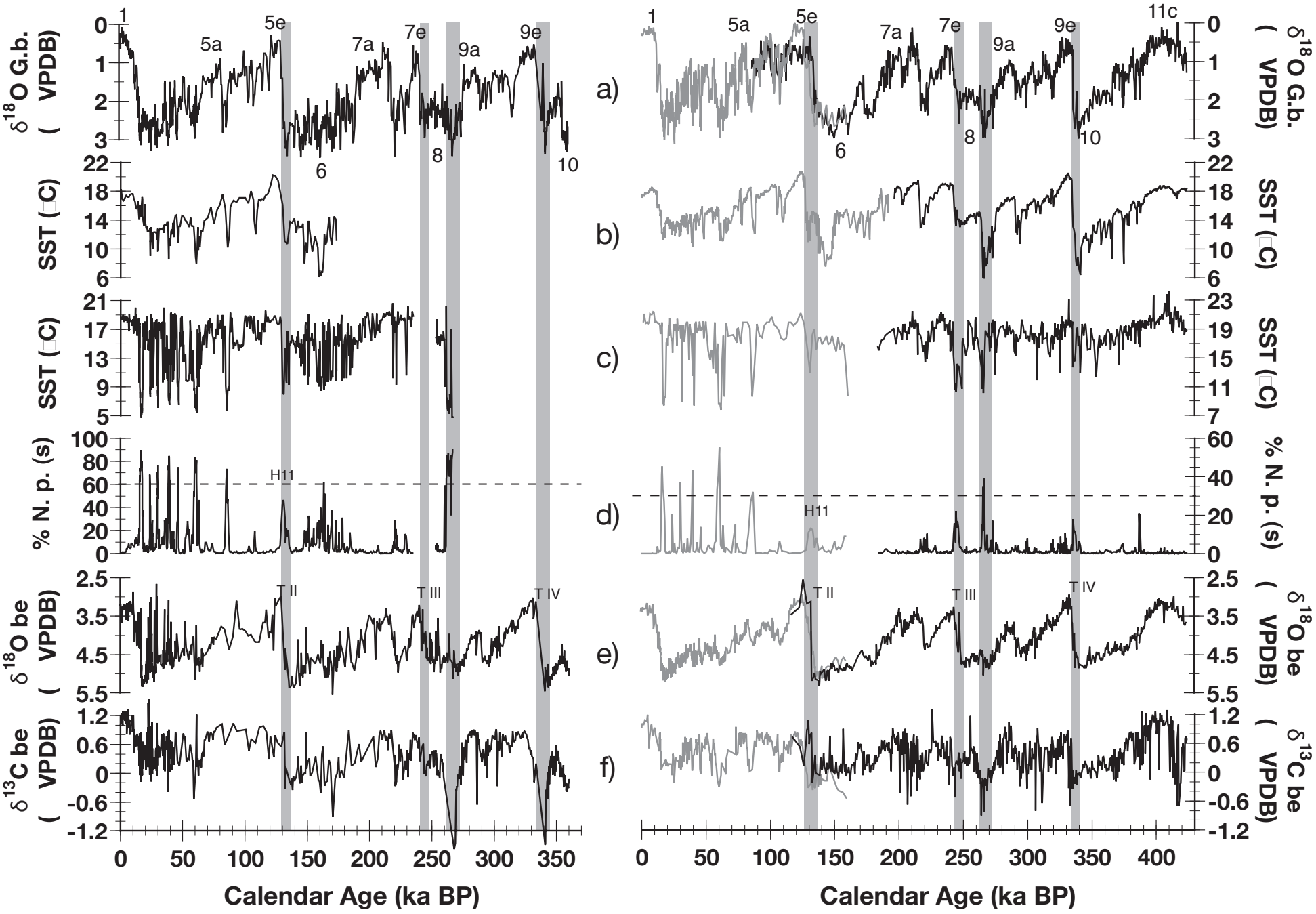
MD95-2040 (40.6°N)
MD95-2042/ MD01-2444/ MD01-2443 (37.9°N)
δ18O G.b. (VPDB)
SST (°C)
SST (°C)
% N. p. (s)
δ18O be (VPDB)
δ13C be (VPDB)
1
5a
5e
6
7a
7e
8
9a
9e
10
11c
H11
T II
T III
T IV
a)
b)
c)
d)
e)
f)
Calendar Age (ka BP)
Calendar Age (ka BP)

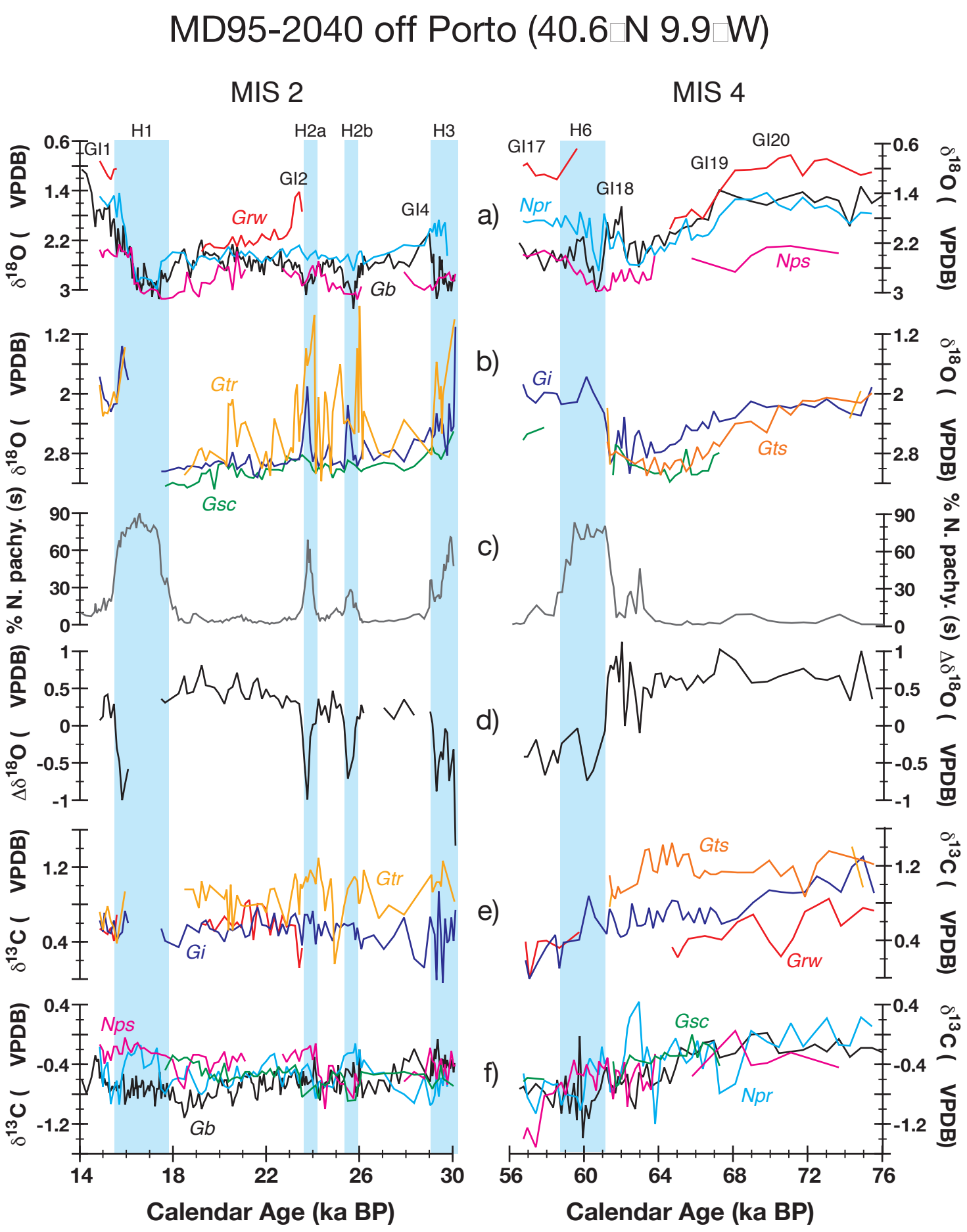

Voelker & de Abreu Figure 6

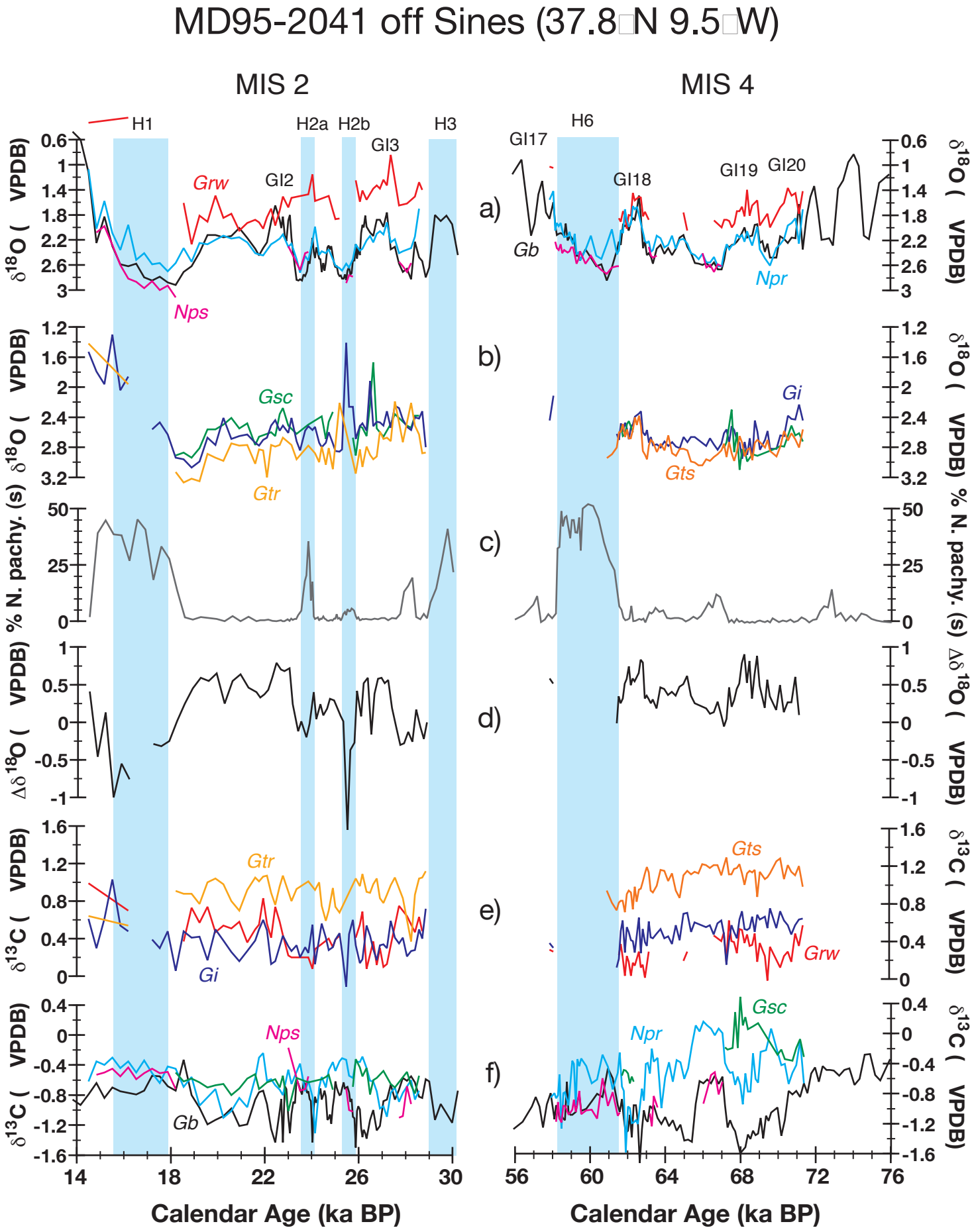

Voelker & de Abreu Figure 7

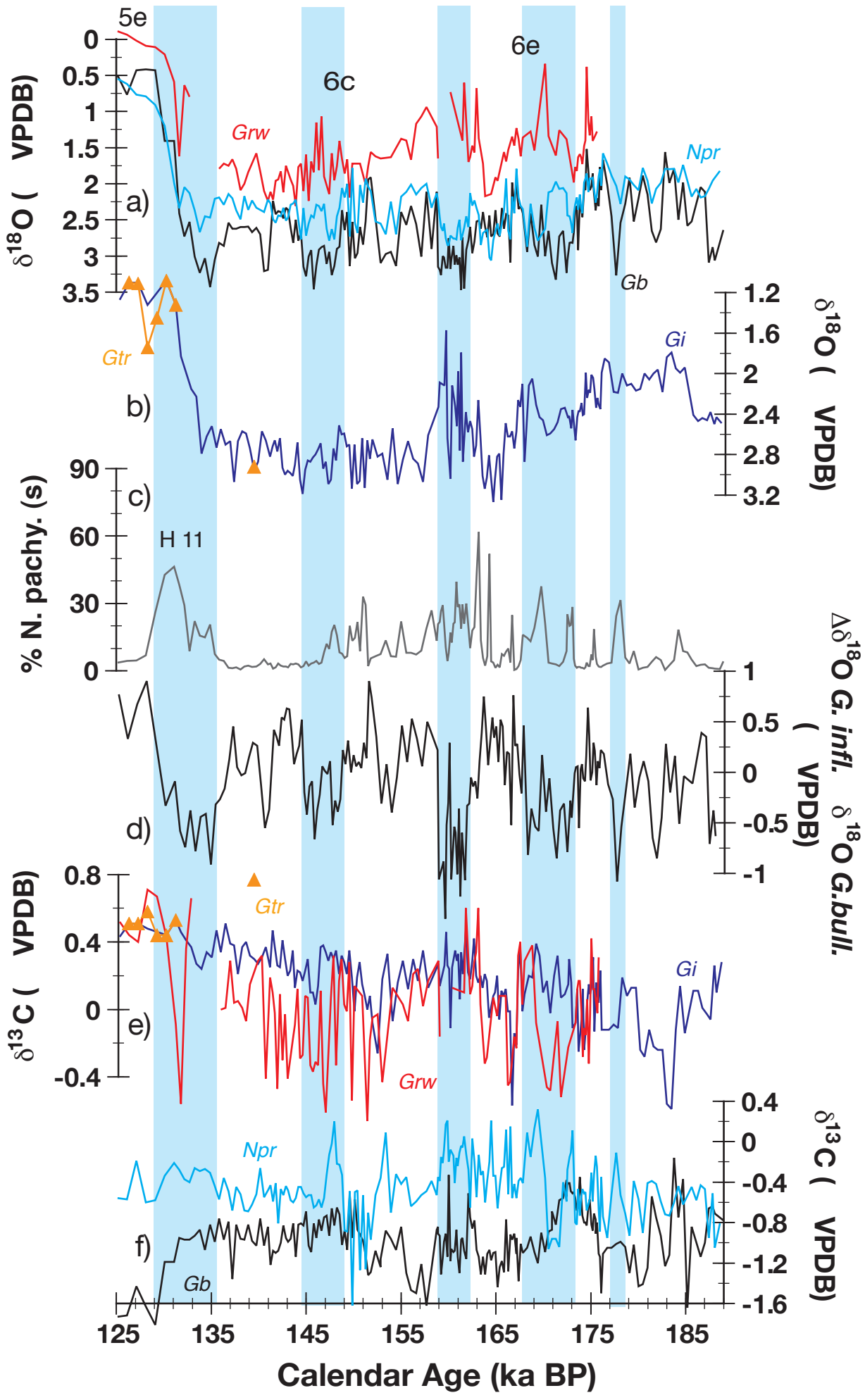
MD95-2040 off Porto (40.6□N 9.9□W)
5e
6c
6e
Grw
Npr
Gb
Gi
Gtr
a)
b)
c)
d)
e)
f)
H 11
δ18O (VPDB)
% N. pachy. (s)
Δδ18O G. infl. δ18O G.bull. (VPDB)
δ13C (VPDB)
Calendar Age (ka BP)
0
0.5
1
1.5
2
2.5
3
3.5
1.2
1.6
2
2.4
2.8
3.2
90
60
30
0
1
0.5
0
-0.5
-1
0.8
0.4
0
-0.4
0.4
0
-0.4
-0.8
-1.2
-1.6
125
135
145
155
165
175
185

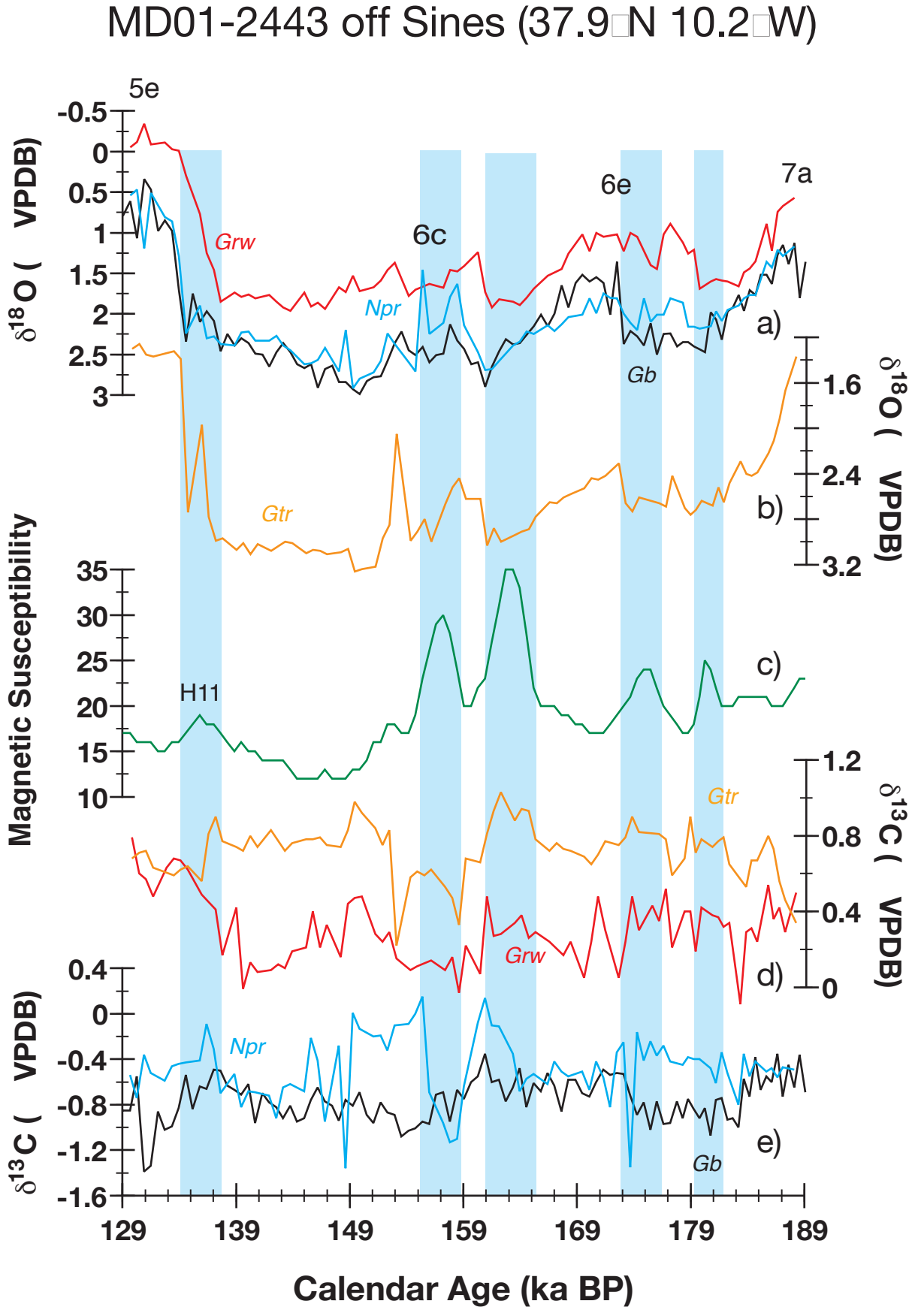

Voelker & de Abreu Figure 9

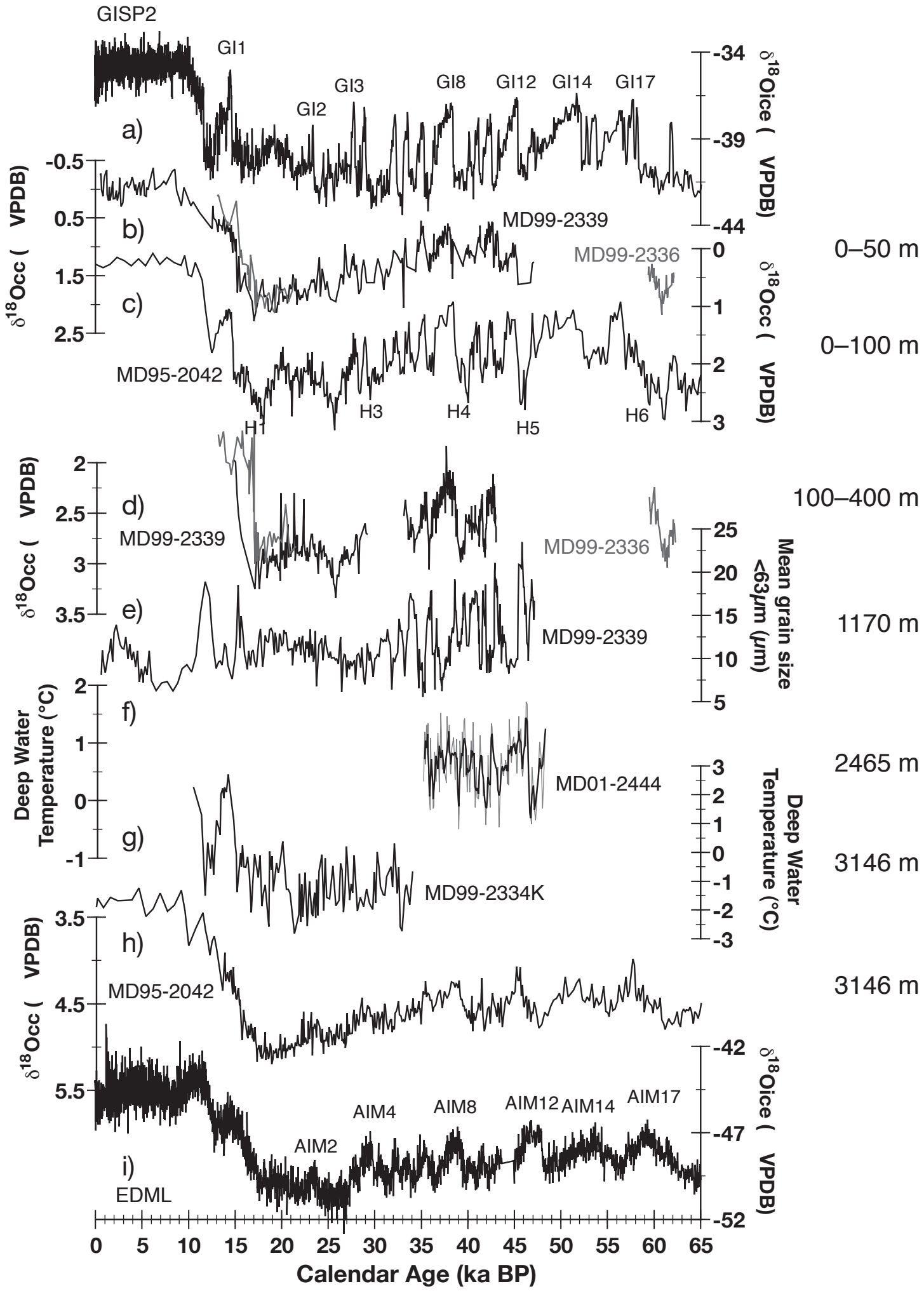
GISP2
GI1
GI2
GI3
GI8
GI12
GI14
GI17
a)
δ18Oice (VPDB)
-34
-39
-44
-0.5
0.5
1.5
2.5
δ18Occ (VPDB)
b)
MD99-2339
MD99-2336
c)
MD95-2042
0
1
2
3
δ18Occ (VPDB)
0–50 m
0–100 m
H1
H3
H4
H5
H6
d)
MD99-2339
MD99-2336
e)
MD99-2339
100–400 m
1170 m
Mean grain size <63μm (μm)
25
20
15
10
5
Deep Water Temperature (°C)
f)
MD01-2444
g)
MD99-2334K
2465 m
3146 m
3
2
1
0
-1
-2
-3
Deep Water Temperature (°C)
h)
MD95-2042
3146 m
AIM2
AIM4
AIM8
AIM12
AIM14
AIM17
i)
EDML
-42
-47
-52
δ18Oice (VPDB)
0
5
10
15
20
25
30
35
40
45
50
55
60
65
Calendar Age (ka BP)

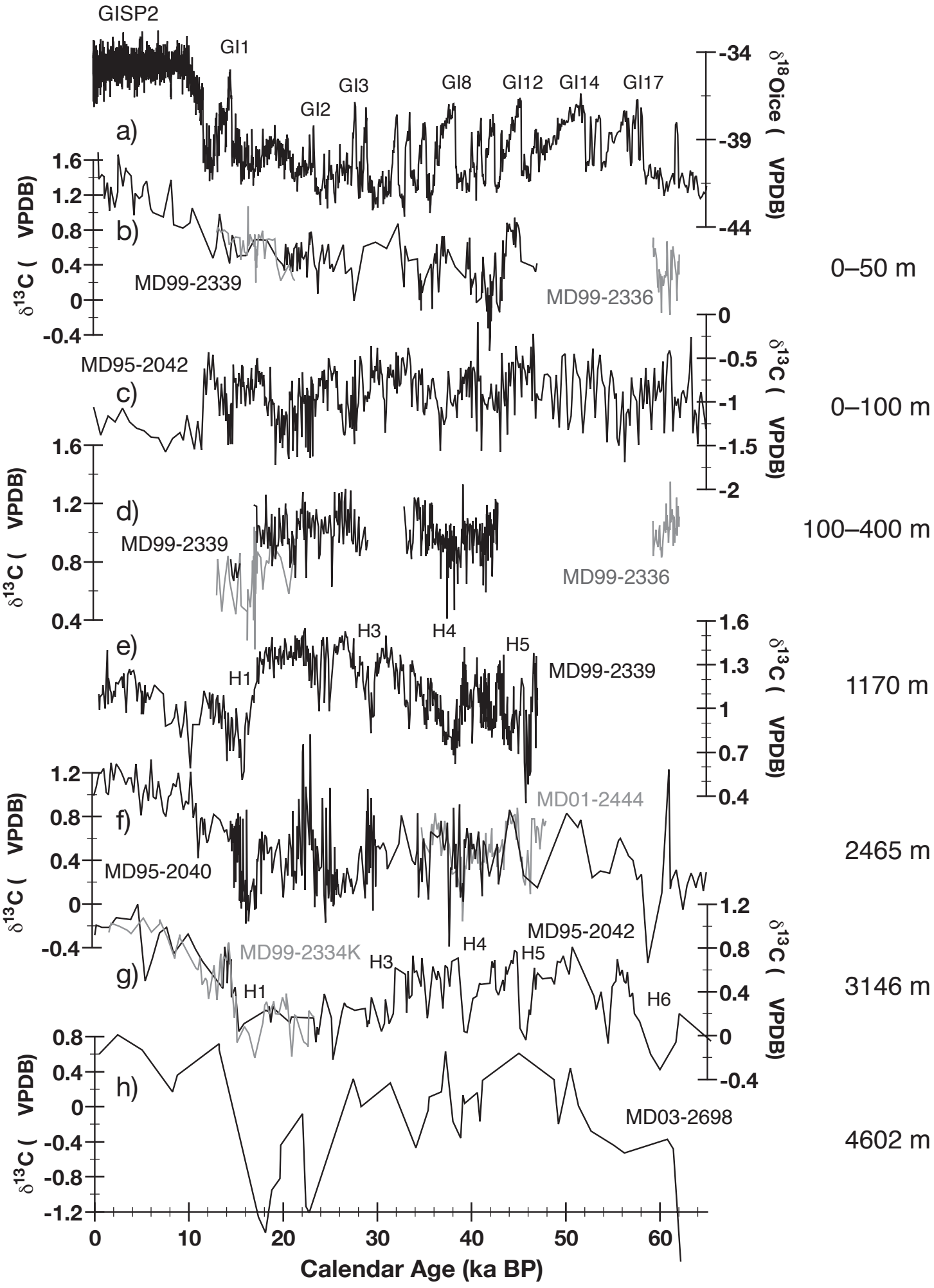
GISP2
GI1
GI2
GI3
GI8
GI12
GI14
GI17
a)
δ18Oice (VPDB)
-34
-39
-44
b)
δ13C (VPDB)
MD99-2339
MD99-2336
0–50 m
MD95-2042
c)
0–100 m
d)
100–400 m
H1
H3
H4
H5
e)
1170 m
MD01-2444
f)
MD95-2040
2465 m
MD99-2334K
MD95-2042
H6
g)
3146 m
h)
MD03-2698
4602 m
0
10
20
30
40
50
60
Calendar Age (ka BP)